Negative thermal expansion near the precipice of structural stability in open perovskites

Connor A. Occhialini [1,2a], Gian G. Guzmán-Verri [3,4b],

Sahan U. Handunkanda[1,2] and Jason N. Hancock [1,2c]

[1] *Department of Physics, University of Connecticut, Storrs, Connecticut 06269, USA,*

[2] *Institute of Materials Science, University of Connecticut, Storrs, Connecticut 06269, USA*

[3] *Centro de Investigación en Ciencia e Ingeniería de Materiales (CICIMA), Universidad de Costa Rica, San José, Costa Rica 11501 and*

[4] *Materials Science Division, Argonne National Laboratory, Argonne, Illinois 60439, USA*

(Dated: September 28, 2018)

Negative thermal expansion (NTE) describes the anomalous propensity of materials to shrink when heated. Since its discovery, the NTE effect has been found in a wide variety of materials with an array of magnetic, electronic and structural properties. In some cases, the NTE originates from phase competition arising from the electronic or magnetic degrees of freedom but we here focus on a particular class of NTE which originates from intrinsic dynamical origins related to the lattice degrees of freedom, a property we term *structural* negative thermal expansion (SNTE). Here we review some select cases of NTE which strictly arise from anharmonic phonon dynamics, with a focus on open perovskite lattices. We find that NTE is often present close in proximity to competing structural phases, with structural phase transition lines terminating near T=0 K yielding the most superlative displays of the SNTE effect. We further provide a theoretical model to make precise the proposed relationship among the signature behavior of SNTE, the proximity of these systems to structural quantum phase transitions and the effects of phase fluctuations near these unique regions of the structural phase diagram. The effects of compositional disorder on NTE and structural phase stability in perovskites are discussed.

Keywords: Negative thermal expansion; Structural negative thermal expansion; Quantum phase transition; Structural phase transition; Perovskite; Antiferrodistortive phase transition; Scandium trifluoride

[a] Present affiliation: Department of Physics, Massachusetts Institute of Technology, Cambridge, MA 02139, USA

[b] Email: gian.guzman@ucr.ac.cr

[c] Email: jason.hancock@uconn.edu

I. INTRODUCTION

Thermal expansion is among the most widely recognized thermodynamic properties of materials. From a textbook perspective[1], thermal expansion occurs through anharmonic free energy terms arising from nuclear lattice degrees of freedom. The dominant appearance of the positive thermal expansion (PTE) found in both research-grade and industrial materials is heuristically ascribed[2–4] to the expected anharmonic behavior of a generic interatomic potential, which is hard at short distance and soft at large distance (Figure 1a). As temperature is raised, higher energy excitations are populated which have an ever increasing mean separation, dilating the bond and presumably lattice dimensions. Of course this is not a theorem any more than crystals are molecules and collective motion of lattices permit various potential landscapes, such as a librational coordinate of tetrahedral molecular solids[5], which possess clear qualitative differences (Figure 1b).

Mention of negative thermal expansion (NTE), a material's tendency to shrink when heated, often evokes discussion of liquid water-ice expansion responsible for icebergs and the 4K temperature window above the ice-water phase boundary where phase fluctuations occur. This is an example of a route to achieving NTE which relies on broadened phase transitions between a low-temperature high-volume phase fluctuating into a high-temperature low-volume phase, other examples of which include the industrial alloy InVar[7] ($Fe_{64}Ni_{36}$) and more recently discovered NTE materials[8–12] (for more details on this approach, see Takenaka's review in this volume[13]). While this route to realizing NTE is promising for many applications requiring only dimensional concerns, NTE at these broadened transitions occurs only in heavily restricted regions of the magnetic and electronic phase diagrams, constraining a thermodynamic number of degrees of freedom to achieve a single mechanical characteristic. Thus, these types of NTE materials will be severely restricted in their potential for multifunctional applications.

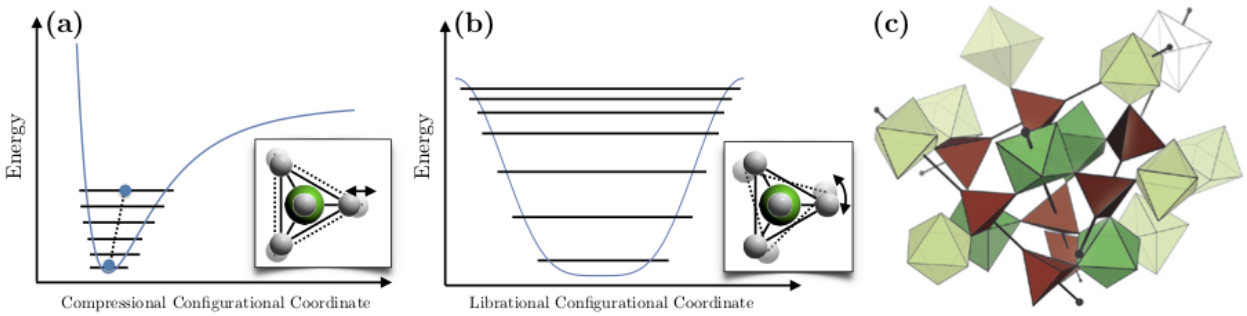

FIG. 1. Intermolecular potentials provide a heuristic explanation for the common occurrence of (a) PTE and (b) NTE. (c) The complex structure of the low-symmetry α-phase of ZrW_2O_8, from Ref. [6].

Remarkably, there exists a growing class of materials with strong, isotropic, robust, and thermally persistent NTE that arises from structural motifs[14–48]. NTE in these systems is often discussed in connection with transverse fluctuations of a linkage between volume-defining vertices, which may accompany the librational, or hindered rotational motion of polyhedral subunits. The energy landscape for such motion tends to be much softer (0-2 THz) than bond-stretching motion (10-30 THz in oxides) which is often the implicated culprit of PTE. Here, NTE arises from the cooperative fluctuations of the bond network on THz time scales under very strong anharmonic influences and appears without necessarily constraining the magnetic or electronic phase diagram, permitting one to envisage new multifunctional materials with diverse mechanical, spin, orbital, thermal, electronic, superconducting, and more exotic order coexisting with NTE. Study of the unusual physics behind this type of NTE informs discovery efforts to find new contexts for this remarkable phenomenon. In addition, NTE materials hold promising application potential in stabilizing fiber Bragg gratings for high-speed telecommunication[49,50], substrates for devices which benefit from thermally controlled stresses and the formation of rigid composite structural materials with engineered thermal characteristics through combinations of PTE and NTE components[51–55].

This second circumstance for NTE, which we term *structural* NTE (SNTE), is the focus of the present article. The field of SNTE has been met with sustained interest from the physics, chemistry, and materials science communities since the re-discovery of the strong SNTE in ZrW_2O_8 in 1996[14,44]. The SNTE effect here persists over the temperature range 4-1050 K and has a sizable linear coefficient of thermal expansion (CTE) of $\alpha_\ell \simeq -9$ ppm/K near room temperature, which is isotropic due to the cubic symmetry maintained at all observed temperatures under ambient pressure. The low-symmetry α-phase structure of ZrW_2O_8 (Figure 1c) consists of ZrO_6 octahedra and WO_4 tetrahedra in the $P2_13$ space group, which has a screw axis along [111]. An order-disorder structural transition to a (cubic) $Pm\bar{3}$ γ-phase occurs at zero pressure and $T_c \simeq 450$K. The NTE effect survives the structural transition, with a small discontinuity and reduction in the CTE to $\alpha_\ell \simeq -6$ ppm/K. Furthermore, application of hydrostatic pressure at $T = 300$K first induces an orthorhombic transition at $P_c = 0.3$ GPa, followed by pressure-induced amorphization realized between $P = 1.5 - 3.5$ GPa[15,18,56]. Both the α- and γ-phases contain four formula units, $N = 44$ atoms, in each unit cell, leading to a complex phononic structure with 3 acoustic and $3N - 3 = 129$ optical branches.

Despite decades of intense research, the complex structure and associated dynamics of the ZrW_2O_8 lattice and the related MA_2O_8 compounds complicates the interpretation of both theoretical and experimental investigations into the mechanisms of SNTE. For instance, a commonly identified

feature in the low-temperature α-phase is the two WO_4 tetrahedra with unshared "terminal" oxygen atoms aligned along the screw axis. The under-constrained freedom of these tetrahedra along this axis are often cited as being responsible for the softness of the crucial NTE modes, but there is much debate as to the precise nature of the mode and its contributions to NTE[21,28]. Several attempts at describing the soft mode as either a translation or rotation of the WO_4 polyhedron were addressed via the space group symmetry - both rotational and translational motion are permitted and necessarily coupled due to the lost inversion symmetry. Another level of controversy in ZrW_2O_8 is the extent to which the molecular subunits may be regarded as rigid[23,33,40,41,57]. Although ZrW_2O_8 presents clear scientific challenges, its discovery is significant in that it ignited a flurry of research into the microscopic origins of the SNTE, both theoretical and experimental, employing both thermodynamic[21] and spectroscopic[20,26,28,31] probes of the low-energy lattice behavior. Some essential, guiding observations were revealed during the ensuing years: (i) ZrW_2O_8 has unusually low-energy lattice modes near 2-3meV[21,28], (ii) structural phase transitions are readily induced via light hydrostatic pressure[15,18,56] and (iii) the SNTE arises from a delicate balance of the degrees of freedom and constraint in the host lattice framework[23,33,40,41,57].

One central question motivating SNTE research is why some materials show SNTE and others do not? To address this question will open avenues to discovery of new NTE materials and advancing technology born from its unique properties. While the precise mechanisms behind the dramatic SNTE in ZrW_2O_8 are still under contention, a variety of other simpler systems with equally impressive SNTE have been discovered in recent years[42,58,59]. In moving towards the goal of a deeper understanding of SNTE mechanisms, we sharpen our focus on the growing class of perovskite materials exhibiting NTE, including ScF_3, ReO_3 and related structural family members. We consider the rich structural phase diagrams of the perovskite structure and their description in terms of octahedral tilts and the corresponding slow lattice dynamics associated with the structural transitions. Although numerous, the hierarchy of phases is well understood and documented, making perovskites a particularly simple framework on which to study the interplay of lattice dynamics and macroscopic phenomena like NTE. In particular, we note how the corresponding dynamic modes of the perovskite lattice relate to soft-mode instabilities that accompany the approach to realized and incipient structural phase transitions and how these are coupled to mechanisms resulting in SNTE. Most importantly, we further develop the apparent connection between the emergence of SNTE alongside phase fluctuations that occur near T=0K structural quantum phase transitions (SQPTs), for which we present the available experimental evidence and develop a systematic modeling scheme to explain the coupling between phase fluctuations and thermal expansion anomalies in perovskite

materials.

II. PEROVSKITES, STRUCTURAL PHASES AND SOFT-MODE INDUCED TRANSITIONS

The perovskite lattice structure may well be identified as the double-helix of the solid state - a framework which is highly functionalizable, tunable, robust, and underpins perhaps every known category of physical behavior. This includes high-temperature superconducting, itinerant ferromagnetic, local ferromagnetic, ferroelectric, insulating, metallic, glassy, as well as a plethora of antiferromagnetic and other poorly understood phases which appear to compete, coexist, and cooperate within typically rich and complex phase diagrams[60–63]. The cubic perovskites are lattice structures with formula unit ABX_3, where the A-site is typically an alkali or alkaline earth metal ion, B is a transition metal and X is the anion, most commonly forming an oxide or a halide. The highest-symmetry solid phase is shown below in Figures 2a and 3a, with a cubic space group symmetry $Pm\bar{3}m$ and the B-site ions in an $n = 6$ octahedral coordination environment of X-site anions. A hierarchy of structural phases in the perovskites are achieved through various concerted rotations of the BX_6 coordination octahedra. These phases have been cataloged and a relationship between octahedral tilts and the lower-symmetry space groups due to these structural distortions have been developed[64,65] and are well-known in the ferroelectric community[66].

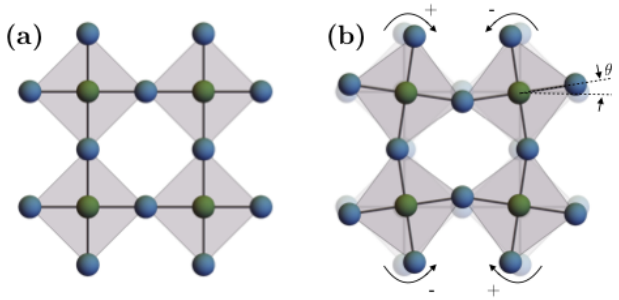

FIG. 2. (a) A single 2D layer of perovskite octahedra in the high-symmetry cubic phase, viewed along one of the 3 fourfold axes and (b) the same layer with a non-zero tilt angle θ, showing the constrained motion of neighboring octahedra due to shared inter-octahedral X-sites.

The scheme for indexing the possible octahedral tilts begins with a 2x2x2 unit cell of the cubic $Pm\bar{3}m$ perovskite and considers rotations of the octahedra about each of the 3 fourfold (C_4) axes of the cubic phase. In the plane normal to a given rotation axis, neighboring octahedra are constrained to rotate at equal angles (θ) of opposite sign, since neighboring B-sites are bonded to a common

X-site anion (Figure 2b); there is, however, a choice in the phase of rotations for columns of octahedra along the rotation axis. Which phase pattern is realized is denoted by a superscript of $+$ or $-$ for in- and out-of-phase stacking, respectively, or a superscript of 0 indicating a null rotation. The equality of rotation angles around each axis is given by using repeated characters. For instance, in Glazer notation $a^+b^+c^+$ represents three unequal rotations about [100], [010] and [001], with all rotations in phase along each respective axis. Overall, there are 23 distinct possibilities of perovskite space groups and octahedral tilting patterns, which can be cubic to triclinic and anything in between. Several relevant examples of perovskite distortions and the Glazer notation are given in Figure 3.

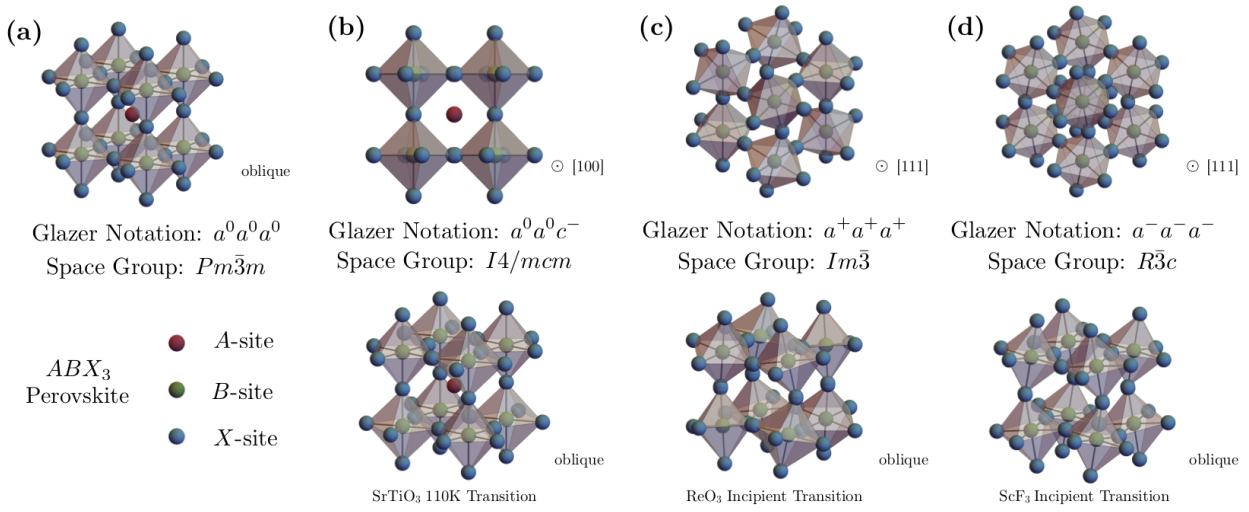

FIG. 3. Shown here is (a) the general perovskite structure of formula unit ABX_3 (see text), in the highest symmetry cubic space group $Pm\bar{3}m$ corresponding to a Glazer tilt notation $a^0a^0a^0$. Also shown are common octahedral tilt lower-symmetry perovskites found in (b) the $SrTiO_3$ $T_c = 110$K $Pm\bar{3}m$ to $I4/mcm$ tetragonal structural transition (c) the triply degenerate M_3^+ phonon condensation in the low-T, high-P ReO_3 structural transition (see text) and (d) the triply degenerate R_4^+ phonon condensation responsible for the rhombohedral transition is BF_3 open perovskite $3d$-transition metal trifluorides which also acts as the dynamic soft-mode rotations in ScF_3, corresponding to Glazer tilts of $a^0a^0c^-$, $a^+a^+a^+$ and $a^-a^-a^-$, respectively.

One of the best-studied structural instabilities in a perovskite structure is the transition at $T_c \simeq 110$K in $SrTiO_3$, first identified with electron spin resonance (ESR) spectra by Unoki and Sakudo[67] and later confirmed by many others[68–71] via inelastic neutron scattering (INS), X-ray diffraction and Raman spectroscopy (RS). The room-temperature structure of $SrTiO_3$ is that of the common $Pm\bar{3}m$ space group depicted in Figure 3a, but signatures of tetragonal symmetry in the ESR and Raman[71] spectra are observed below $T \simeq 110$K, along with anomalies in the elasticity[72].

Details of the atomic displacements reveal the lower-symmetry structure is the tetragonal $I4/mcm$ space group, which corresponds to a [001]-phase-staggered rotation of the TiO_6 octahedra about a [001] rotation axis, that is an octahedral tilting pattern of $a^0a^0c^-$ (Figure 3b). The displacements are related to the polarization of a zone-boundary optical phonon (irrep. R_{25}) existing at the R-point of cubic Brillouin zone (BZ) (Figure 4a). In real space, the lowered-symmetry results in an effective doubling of the unit cell dimensions along one axis. In reciprocal space, however, the symmetry lowering occurs through a halving of the Brillouin zone and results in formation of new Bragg peaks as seen in an elastic scattering pattern (X-ray, neutron, electron). Dynamically, one can associate the transition to a slowing down of an optical phonon near the R ($\pi\pi\pi$) point at the corner of the cubic Brillouin zone, corresponding to a "freezing" or "condensation" of one component of the triply degenerate R-point "soft" mode.

$SrTiO_3$ is the first material in which soft modes were measured using inelastic scattering, and their concomitance with structural phase transitions was subsequently established through their observation in many other perovskites, e.g. $LaAlO_3$, $KMnF_3$, $PbTiO_3$ and $BaTiO_3$[73]. A *soft-mode* can generally be defined as any normal mode of the dynamic lattice whose energy or, equivalently, frequency of vibration decreases anomalously. When such a vibrational frequency reaches $\hbar\omega = 0$, the lattice becomes structurally unstable with respect to the displacements of this normal mode, and a subsequent symmetry-lowering, static deformation occurs to restore stability. For the simplest case of Landau-Ginsburg-Devonshire theory treated at the mean-field level, one expects a temperature dependence for the soft mode frequency[73–75]:

$$\omega_s(T) \propto \sqrt{|T - T_c|} \tag{1}$$

This dependence for the R-point soft-mode in $SrTiO_3$ is shown in Figure 4b. This transition can be described by an order parameter, a quantity that is zero above and develops non-zero average values below T_c, which follows the angle of rotation of the TiO_6 octahedra about the principal axis in the low-symmetry tetragonal structure. The transition in $SrTiO_3$ is, by all experimental accounts, second-order (continuous) in nature, but for many structural phase transitions signatures of the more common first-order (discontinuous) behavior renders the soft-mode approach invalid *a priori*. Nonetheless, soft modes can be used to interpret weakly first-order transitions and their frequency can be indicative of an incipient transition due to soft-mode coupling to other, primary order parameters. The 110K transition in $SrTiO_3$ is also a prototypical example of critical behavior that can emerge in the vicinity of a structural transition, most notably the "central-peak" phenomenon

discovered through an anomalous quasi-elastic peak in INS energy-transfer spectra, which can be explored elsewhere[76–78].

In extreme cases, a material can approach dynamic instability with lowering temperature to near-zero soft mode energy, yet no temperature-induced transition is observed. In this situation, subsequent application of pressure, introduction of compositional disorder (doping) or other non-thermal parameters can perturb the ground-state of the system to drive the transition at $T = 0$K, realizing a quantum phase transition (QPT)[79]. Research surrounding the breakdown of canonical physical behavior near these quantum critical points (QCPs) is interesting in its own right[80,81] but we below focus on QCPs within the structural phase diagrams and their relationship to the development of SNTE in a subset of the perovskites.

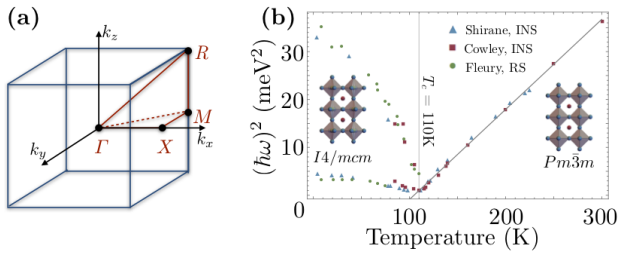

FIG. 4. (a) The cubic Brillouin zone indicating the high-symmetry reciprocal lattice points Γ, X, M and R. (b) R-point mode softening on the approach to the $T_c \simeq 110$K structural transition in $SrTiO_3$, measured from neutron[68,70] and Raman[71] scattering. Black line for $T \geq T_c$ shows agreement with the predicted soft-mode frequency for a dynamically driven second-order phase transition as given in Eq. 1.

III. NTE IN PEROVSKITE FRAMEWORKS

Most oxide perovskites ABO_3 form with an A-site, otherwise requiring a rare hexavalent electronic configuration for charge balance. One prominent exception is ReO_3, which forms with no A-site and maintains its cubic $Pm\bar{3}m$ space group symmetry down to the lowest measured temperatures. In addition, ReO_3 has been known to exhibit SNTE for many years, which is often attributed to soft modes permitted by the open-perovskite (A-site-free) structure. The lack of the A-site puts fewer dynamical constraints on the motion of the ReO_6 octahedra in comparison to the constraints imposed by the A-site in other perovskites. This permits large anisotropic thermal displacements of the linking oxygen atoms perpendicular to the Re-O-Re bond direction, making ReO_3 more susceptible to lattice instabilities corresponding to these octahedral tilt patterns. This openness to the structure has also been noted as a key feature in many other SNTE materials, including

ZrW_2O_8, leading to a larger set of soft, low-energy phonons that have mainly been identified as the cause of SNTE. Reports on the size of the SNTE effect in ReO_3 vary, but in one report, SNTE was observed in two separated temperature windows of 2 - 220 K and 600 - 680 K[82] with a maximum measured linear thermal CTE of $\alpha_\ell = -2.56$ ppm/K[83] (Figure 5).

ReO_3 undergoes several structural phase transitions under hydrostatic pressure and is most studied at room temperature. Early INS investigations at ambient temperature established that ReO_3 undergoes a pressure-induced second-order phase transition at $P_c = 0.52$ GPa[85]. Further studies of transport at $T = 2$ K showed that the lowest structural phase boundary terminates at a light hydrostatic pressure of only $P_c = 0.25$ GPa, observed through a change of Fermi surface cross section[86]; however, few reports are available in this difficult P-T region. Based on early high-temperature data, the pressure-induced phase is likely the tetragonal $P4/mbm$, although recent indications of a direct transition to a cubic $Im\bar{3}$ phase have also been reported[85,87]. Neutron diffraction at elevated hydrostatic pressures revealed that the $Im\bar{3}$ phase is stable in the pressure range 0.5 to 13.2 GPa, above which the phase changes to the rhombohedral $R\bar{3}c$ space group[88]. The soft mode driving the pressure and temperature induced structural transition between the $Pm\bar{3}m$ and $Im\bar{3}$ cubic phases was shown to be three-component M_3^+ phonon mode involving anti-phase rotation of the neighboring ReO_3 octahedra in an $a^+a^+a^+$ tilt pattern (Figure 3c). The temperature-dependence of the M_3^+ mode frequency as a function of temperature at ambient pressure is shown in Figure 6b, along with a fit to the mean-field result (Eq. 1). This mode is

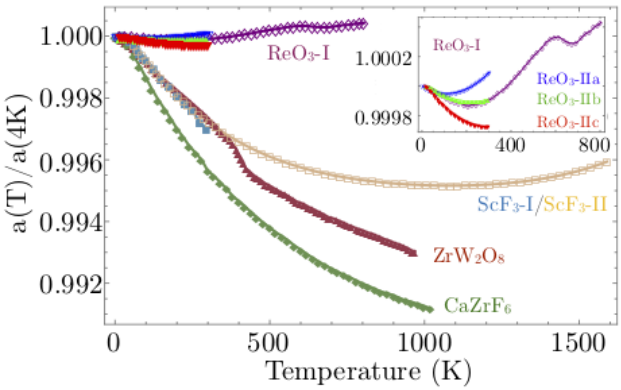

FIG. 5. Shown here is the normalized cubic lattice parameter temperature dependence $a(T)/a(4K)$ for ReO_3, ScF_3 and $CaZrF_6$ NTE perovskites with strong SNTE material ZrW_2O_8 for comparison. Inset focuses on available data for ReO_3 on 4 different samples, one (ReO_3-I) over an extended temperature range[82] and the other 3 (ReO_3-II a-c) over a smaller temperature range, investigating the effects of compositional disorder[58] (see Sec. V). Data taken from: ZrW_2O_8[14], $CaZrF_6$[59], ScF_3-I[84], ScF_3-II[42], ReO_3-I[82] and ReO_3-II[58].

significant in that it is used to understand NTE behavior of open-perovskite systems but is also identified as an order parameter of the phase transition[89].

Unlike oxides, fluorides commonly form stable A-site-free perovskite structures BF_3 due to the wider array of available B^{3+} ion valence configurations among the transition metals. Prominent among these open-perovskite fluorides is ScF_3, which was discovered in 2010 by Greve et al.[42] to exhibit a robust NTE effect, which has significant maximal magnitude of the linear CTE $\alpha_\ell \sim -15$ ppm/K, persisting over the broad temperature range of 4-1050K (Figure 5). At room temperature, ScF_3 crystallizes isostructurally to ReO_3 with space group symmetry $Pm\bar{3}m$ and has been found to possess related structural instabilitiies corresponding to zone-boundary optical phonons. In ReO_3, the condensing soft mode responsible for the low-T high-P structural phase transition is the M_3^+ distortion, while ScF_3 and other $3d$-transition metal trifluorides fall into the lower-symmetry rhombohedral $R\bar{3}c$ space group symmetry, attributed to the condensation of the R_4^+ optical phonon.

Although the cubic phase of ScF_3 is stable at ambient pressure over the entire temperature of the solid phase down to $T = 0.4$K[90], X-ray diffraction[42,91] and Raman spectroscopy[91] results have revealed that ScF_3 undergoes several pressure-induced phase transitions. The first is from cubic to rhombohedral (c-r) after $P_c = 0.6$ GPa at T=300K, with a subsequent rhombohedral to orthorhombic transition occurring above $P_c = 3.0$ GPa. The c-r transition has an observed pressure dependence of $dT_c/dP \simeq 525$ K/GPa[42,91,92]. Measurement of the lattice dynamics and the soft R_4^+ mode responsible for the rhombohedral transition were performed using inelastic x-ray scattering (IXS), which revealed a 1D manifold of soft optical phonons that circumscribe the entire cubic Brillouin zone-edge. At room temperature, this manifold of modes along M-R have energy $\hbar\omega \simeq 3$ meV, softening nearly uniformly to < 1 meV at cryogenic temperatures (see Figure 6b)[84]. The IXS results combined with structural data permit an estimation that pressures as small as $P_c \simeq 0.074$ GPa would be sufficient to drive the transition to 0 K. The sensitivity of the phase boundary suggests that the nature of the cubic phase is delicate at low temperature and has been shown to be susceptible to even mild perturbations[93–95], implying that the ground state of this ionic insulator lie in close proximity to a SQPT.

Phase stability and thermal expansion effects in the open-perovskite trifluoride structure have also been investigated thoroughly through chemical substitution. Chemical substitutions of Sc by Ti[94], Al[95], and Y[93] have been reported and the effects of this compositional disorder will be discussed in detail in Sec. IV and V. Other investigations of changing the stoichiometry have resulted in a related class of hexafluoride compounds, one of which is $CaZrF_6$. This material has $Fm\bar{3}m$ space group symmetry and is related to the $Pm\bar{3}m$ structure of ReO_3 but with a staggered

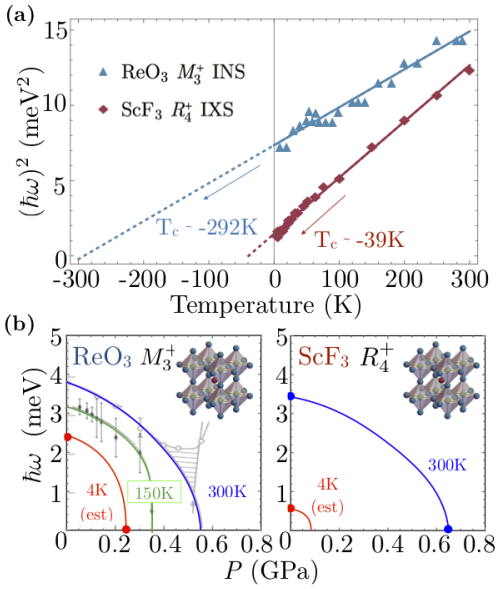

FIG. 6. (a) Shows the squared energy $(\hbar\omega)^2$ of the M_3^+ and R_4^+ soft modes vs. temperature at ambient pressure in ReO_3 and ScF_3, respectively. As indicated, extrapolation by mean-field approximation (Eq. 1) indicates structural transition temperatures at ambient pressure of $T_c \simeq -292$K for ReO_3 and $T_c \simeq -39$K for ScF_3. Figure (b) shows the soft mode energy versus pressure at various temperatures for (left) the M_3^+ mode in ReO_3 and (right) the R_4^+ mode in ScF_3. Solid lines are guide to the eye and symbols in both (a) and (b) are taken from references[84,85,89]. Comparison supports our assignment that ScF_3 is closer to a SQPT than ReO_3.

B-site ion; that is, alternating CaF_6 and ZrF_6 octahedra tiling a simple cubic point-group structure. The resultant $(\pi\pi\pi)$ pattern is likely a key feature when attempting to relate these materials, and is in particular likely to impact the (simple cubic) M-R BZ edge mode dispersion and dimensional reduction observed in ScF_3[84]. Compared to ScF_3, this system has isotropic NTE of larger magnitude $\alpha_\ell \simeq -18$ ppm/K over a temperature range $> 1050K$ (Figure 5). At $P = 0$ the system also remains cubic at all temperatures above 10 K but a pressure-induced transition to a disordered state occurs near $P_c = 0.45$ GPa[59], closer in the P-T diagram than the c-r transition in ScF_3 (~ 0.6 GPa)[42,91,96]. Early computational work suggests the $\Gamma - X$ manifold in the cubic BZ for this compound contribute most strongly to NTE[97], but inelastic scattering measurements of the phonon dynamics are needed to assess the influence of the staggered substitution on the critical SNTE dynamics.

The open-perovskites presented above demonstrate this frameworks' favorable environment for harboring SNTE, but begs the question of why most other purely stoichiometric transition metal trifluorides and perovskites show more conventional thermal expansion. The lattice parameters of each of these SNTE perovskites are plotted in comparison to the prototypical SNTE material

ZrW_2O_8 in Figure 5, which gives a clear ranking of SNTE perovskites by the magnitude of the NTE effect ((1) $CaZrF_6$, (2) ScF_3, (3) ReO_3). This ranking is the opposite ordering one gets in terms of pressure required to induce the structural phase transition nearest ambient conditions, a correlation suggestive that proximity to a SQPT and strength of NTE are interrelated. We demonstrate this point for ReO_3 and ScF_3 in Figure 6. These plots consider the soft-mode in each system, the M_3^+ phonon in ReO_3 and the R_4^+ in ScF_3 and the available data for the energy of these modes as a function of pressure and temperature. First considering the T-dependent data at $P = 0$ in Figure 6a, extrapolation of the squared mode energies by Eq. 1 provides a quantitative measure of the proximity to a dynamically-driven SPT, yielding $T_c \simeq -292$K in ReO_3[89] and $T_c \simeq -39$K in ScF_3[84]. Furthermore, isothermal measurements of the soft-mode energy versus hydrostatic pressure are provided in Figure 6b, showing that decreasing temperature and increasing pressure in both systems trend towards a QCP.

Together, the results of these data clearly show in all respects that ScF_3 is closer to a SQPT than ReO_3. Although data at this level in unavailable for $CaZrF_6$, the amorphization boundary at $P_c \leq 0.45$ GPa and $T = 300$K is a lower pressure threshold for the pressure-induced transitions at 300K in both ReO_3 (~ 0.55 GPa) and ScF_3 (~ 0.65 GPa). It is thus likely that ground-state of this compound is the closest to a structural instability at cryogenic temperature, while also exhibiting the most superlative SNTE effect in this class. Our central hypothesis in the context of the materials described is that the $T = 0$K termination of a structural phase boundary defines a structural quantum critical point (SQCP) where strong geometrical fluctuations associated with octahedral tilts drives NTE. In our view, the significance of the SQCP is a flattening of the energy landscape with respect to transverse fluctuation of the linkage unit: O in ReO_3, and F in ScF_3 and $CaZrF_6$. It is worth noting that NTE arising from phase fluctuations and the displacements of a low-T soft-mode is not unique to the antiferrodistortive (zone-boundary) phonons in perovskites, but has also predicted SNTE in materials with broadly distinct structures and geometrical motifs, e.g. the Hg dimer in Hg_2I_2[98], the CN molecule in Prussian blue analogs and related compounds[99–101].

NTE is often understood through the response of the phonon spectrum to the application of hydrostatic pressure, which has been formalized in the quasi-harmonic approximation (QHA) known as the Grüneisen approach[1]. Each phonon in the Brillouin zone of frequency and wavevector $(\omega_i, \boldsymbol{k}_i)$ is assigned a mode Grüneisen parameter γ_i, defined as,

$$\gamma_i \equiv -\frac{\partial \ln \omega_i}{\partial \ln V} \equiv \frac{1}{\kappa}\frac{\partial \ln \omega_i}{\partial P} \tag{2}$$

where κ is the isothermal compressibility. Performing an average over all $\mathbf{k}$, weighted by the

mode contribution to the heat capacity $c_{V,i}$, gives the overall lattice Grüneisen constant γ which is thermodynamically proportional to the volumetric thermal expansion α_V for isotropic materials. At low-temperatures, the thermodynamic properties are dominated by contributions from the lowest energy excitations. If the low-energy phonon spectrum has large magnitude, negative mode Grüneisen parameters (negative contributions to CTE), then the **k**-averaged CTE will decrease as temperature is lowered. If strong enough to overcome the many high-energy excitations commonly attributed to conventional PTE, the overall expansion may turn negative in sign, strengthening at lower temperature, which is the typical functional form among the SNTE perovskites (Figure 5), before relaxing and limiting to a thermodynamically-required $\alpha_V = 0$ as $T \to 0$K. From this viewpoint, soft-modes with NTE contributions are natural candidates for inducing overall NTE, since their energy softens with lowering temperature, enhancing the mode occupation and weighted contributions to the thermodynamics at low-T in comparison to thermally-stable low energy excitations.

In the SNTE perovskites and other SNTE materials like ZrW_2O_8, these lowest energy lattice excitations are commonly attributed to quasi-rigid dynamics of polyhedral subunits[57], i.e. the geometrically rigid octahedra as shown in Figure 2 which could correspond to BX_6 octahedra in ScF_3, ReO_3 or $CaZrF_6$. These rigid unit mode (RUM) analyses model rigidity by freezing out portions of the phonon spectrum, such as high-energy bond-stretch and internal polyhedral bond-bend modes that are commonly attributed to causing PTE. For ScF_3 and ReO_3, the antiferrodistortive, zone-edge soft modes have an interpretation as RUMs. Moving beyond the commonly employed QHA and Landau mean-field approaches, we make the hypothesized relationship among soft RUMs, phase fluctuations and the development of SNTE precise within a systematic model in Sec. IV below.

IV. THEORY OF SNTE FROM RUM FLUCTUATIONS

The purpose of this section is to present a microscopic description of NTE arising from soft modes in ReO_3-type lattice structures. Such modes break the symmetry of the lattice and lead to displacive structural phase transitions[102]. Typical examples are the R_4^+ mode at the point $(1,1,1)\,(\pi/a)$ of the Brillouin zone of the cubic (c) $Pm\bar{3}m$ phase in MF_3 (M=Sc, Al, Cr, V, Fe, Ti) metal fluorides which upon condensation gives rise to a rhombohedral (r) $R\bar{3}c$ lattice structure and the M_3^+ mode at $(1,1,0)\,(\pi/a)$ in ReO_3 which generates a tetragonal ($P4/mbm$) phase.

The structural transitions observed in these materials are generally described by Landau

theories[85,103]. Typically, they include an order parameter (OP) associated with cooperative tilts of a rigid unit (e.g. the MF_6 octahedron in the metal fluorides) coupled to long-wavelength acoustic phonons that generate volume, deviatoric and shear strains. While such mean field theories provide a fair description of the structural transitions, they fail to describe NTE, e.g., they predict zero thermal expansion in their high-T cubic $Pm3m$ phase.

Here, we present a microscopic phenomenology that describes NTE in these open perovskite frameworks. The model includes the usual rigid tilts coupled to long-wavelength strain-generating acoustic modes as well as a cooperative interaction between tilts that drives the structural transition, e.g., dipolar interactions in the metal trifluorides[104–106]. Our main result is that any solution of the model must include fluctuations of the OP to generate NTE. We illustrate this within a so-called self-consistent phonon approximation (SCPA) in which single site fluctuations are considered while inter-site fluctuations are neglected. This point has been appreciated before[107], however, no systematic approach has been constructed so far. In addition, our model allow us to parametrize measured macroscopic quantities in terms of microscopic parameters, which provides guidance for materials design. Our model closely follows those of the well-known antiferrodistortive transitions of $SrTiO_3$ and $LaAlO_3$[108], with the important distinction that we include hydrostatic pressure and account for compositional disorder. The latter is aimed at describing compounds with tunable NTE through composition such as mixed solid solutions of metal triflurides[43,94,95]. For concreteness, we will consider a c-r transition similar to that in $Sc_xTi_{1-x}F_3$ in which the threefold zone-boundary R_4^+ phonon splits into a low-energy E_g doublet and a high energy A_{1g} singlet at a transition temperature T_c[109].

Our model analysis is by no means exhaustive. More elaborate descriptions that go beyond the picture of rigid tilts involving, for instance, distortions and translations of such building units are usually needed to describe the observed TE[110]. Also the observed structural transitions are frequently of first-order, which we do not consider here for the sake of simplicity. Nonetheless, our semi-analytic approach accounts for microscopic aspects of the phonon dynamics and its relation to NTE and help in finding general trends of the solution. Moreover, it provides the basis to build other frameworks that capture atomistic details such as first-principles-based effective model Hamiltonians[111].

A. Model Hamiltonian

We consider a cubic lattice with N sites and choose normal mode coordinates $\boldsymbol{Q}_i = (Q_{ix}, Q_{iy}, Q_{iz})$ in the unit cell $i\,(i = 1, 2, ..., N)$ associated with the R_4^+ mode, the condensation of which leads to the $R\bar{3}c$ rhombohedral phase. $\boldsymbol{Q}_i$ is proportional to the local displacements generated by the cooperative tilts of the MF_6 octahedra. In addition, we introduce the strain tensor in Voigt notation $\epsilon_{i\alpha}$, $\alpha = 1, ..., 6$ in unit cell i, which is induced by displacements $\boldsymbol{u}_i = (u_{ix}, u_{iy}, u_{iz})$ of the centers of mass of the unit cells with respect to the acoustic-branch phonons. In order to determine the optical phonon contribution to the thermal expansion, we must couple the displacements $\boldsymbol{Q}_i$ with strains $\epsilon_{i\alpha}$, leading to a 3-term Hamiltonian of the form,

$$H = H_Q + H_\epsilon + H_{Q\epsilon}. \tag{3}$$

Here, H_Q accounts for harmonic and anharmonic energy contributions from the soft optical phonon up to quartic order in $\boldsymbol{Q}_i$; H_ϵ is the strain-induced energy depending on the elasticity through the bulk modulus C_a, shear moduli and hydrostatic pressure P; and $H_{Q\epsilon}$ models the coupling between these displacements and strain degrees of freedom with g_a the coupling constant between the displacements and the volume strain. The explicit form of these terms is given in the supplementary material (SM). To solve the statistical mechanical problem posed by the Hamiltonian in Eq. 3, we use a variational formulation of a SCPA, in which the temperature and pressure dependence of the phonon energies Ω_ν, $(\nu = R_4^+, A_{1g}, E_g)$, displacements, strain order parameters and phase fluctuations are determined self-consistently from the minimization of the free energy[112]. We here focus on the main results. The details of the model Hamiltonian and its approximate solution are given in the SM.

B. Thermal expansion, CTE, and Grüneisen parameters.

We first focus on the volume strain $\langle \epsilon_V \rangle = \langle \epsilon_1 + \epsilon_2 + \epsilon_3 \rangle$, which gives the change in volume with temperature and pressure with respect to a reference volume V_0. We use the notation $\langle .... \rangle$ to denote thermal average. By minimizing the free energy associated with the Hamiltonian in Eq. 3, we find that the volume strain is given as follows,

$$\langle \epsilon_V \rangle = \frac{\Delta V}{V_0} = -\frac{g_a}{C_a} \left\langle |\boldsymbol{Q}|^2 \right\rangle - \frac{P}{C_a}, \tag{4}$$

where $\left\langle |\boldsymbol{Q}|^2 \right\rangle$ is the thermal average of the squared magnitude of the MF_6 tilt. Eq. 4 already illustrates one of the the main points of our work: in a mean-field theory and in the absence of pressure, $\left\langle |\boldsymbol{Q}|^2 \right\rangle = 0$ above T_c; thus fluctuations around the OP must be included to describe NTE. For instance, within the SCPA and for temperatures much greater than the phonon energy, we find that $\left\langle |\boldsymbol{Q}|^2 \right\rangle \propto T$ in the cubic phase and Eq. 4 gives,

$$\frac{\Delta V}{V_0} \simeq \alpha_V T - \frac{P}{C_a}, \qquad \alpha_V = -\frac{3 g_a k_B}{C_a v_R}, \tag{5}$$

where α_V is the CTE at high temperatures and v_R is the strength of the cooperative interaction. Figures 7 (a) and (b) show, respectively, our results for the volume change obtained from Eq. 4 and its CTE ($\alpha_V = d\left\langle \epsilon_V \right\rangle / dT$) in the full temperature range. Model parameters were obtained by fitting to experiments[84,94] and are given in the SM. Despite its simplicity, our model produces the observed trends [84,94]: NTE with a nearly linear T dependence in the c-phase, except near 0 K; PTE in the r-phase; and a discontinuity in α_V at the phase transition. Quantitatively, the model is in good agreement in the c-phase, but α_V is about and order of magnitude less than the observed one in the r-phase. We attribute this to having neglected the first-order character of the transition and additional phonons along the M-R line of the BZ which are known to contribute to the NTE [113].

We note that Eq. 5 gives α_V in terms of the microscopic model parameters. It shows that mechanically compliant materials with low bulk moduli (C_a) and strong strain-phonon couplings (g_a) favor thermal expansion. α_V also increases by weakening the strength of the cooperative interaction v_R at the expense of decreasing the transition temperatures since $T_c \propto v_R$, as it is shown in the SM. It also shows that the sign of this coupling plays an essential role in the thermal expansion: $g_a > 0$ for NTE while $g_a < 0$ for PTE.

Another physically relevant quantity is the the Grüneisen parameter γ_ν associated with each lattice mode $\nu = R_4^+, A_{1g}, E_g$. We find that the temperature and pressure dependence of γ_ν is entirely determined by the phonon energy Ω_ν,

$$\gamma_\nu = -\frac{g_a}{\Omega_\nu^2}, \tag{6}$$

and thus diverges near the c-r transition as $\Omega_\nu \to 0$. This is in agreement with previous analytic work[107] and ab-initio calculations, where large, negative values for $\gamma_{R_4^+}$ have been found for ScF_3 [110,113,114]. Figure 7 (b) shows that $\gamma_\nu^{-1} \propto -|T - T_c|$ at the onset of the phase transition for $x = 0.5, 1.0$ and thus matches the result from Landau theory. For $x = 0$, there is no transition and the deviations from linear behavior are due to zero-point fluctuations.

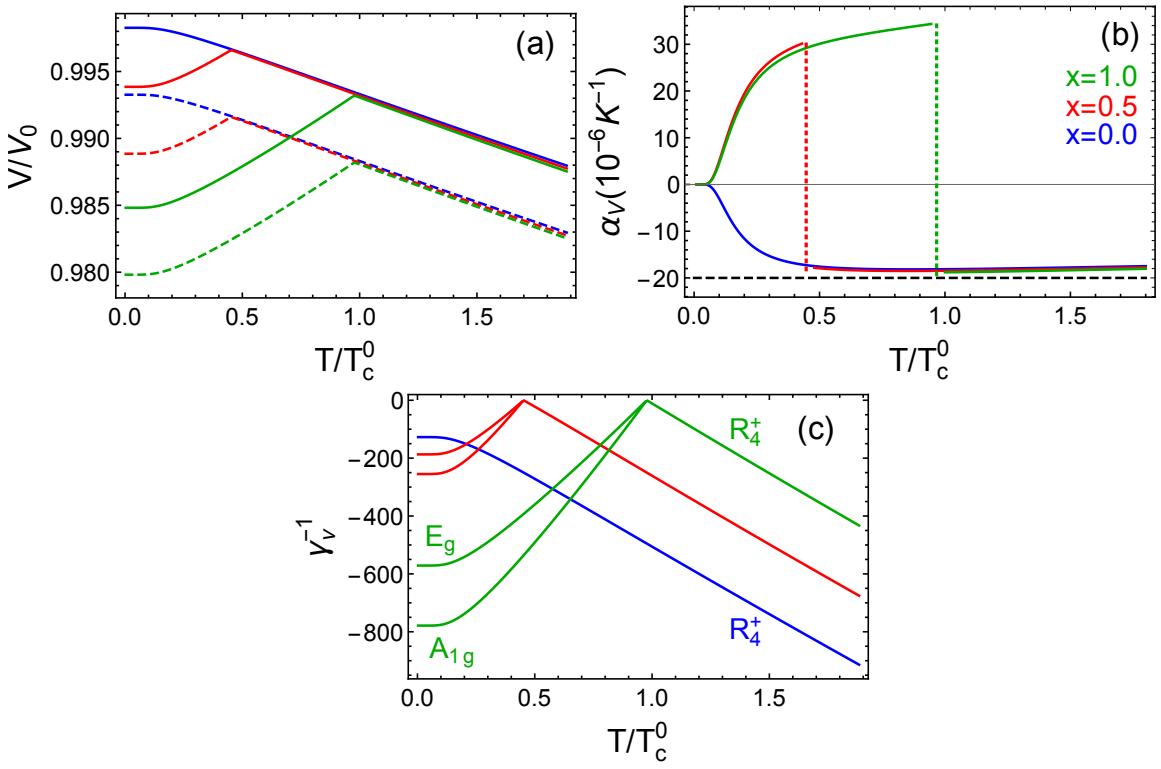

FIG. 7. Calculated temperature dependence of (a) volume change, (b) CTE, and (c) Grüneisen parameters for $P/P_0 = 0$ (solid lines) and 9.0×10^{-5} (dashed lines) for $Sc_{1-x}Ti_xF_3$. P_0 is the pressure needed to induce the c-r transition in ScF_3 ($x = 0$) at 0 K; $T_c^0 = 340$ K is the transition temperature of TiF_3 ($x = 1$) at ambient pressure. Black dashed line in (b) is the predicted CTE in the classical limit according to Eq. (5). The phonon symmetry labels for $x = 0.5$ in (c) are the same as those for $x = 1$ and are not shown for clarity.

V. THE ROLE OF DISORDER IN PEROVSKITE SNTE MATERIALS

Disorder is an inevitable part of any real material system. Here we discuss and develop the role of disorder in on the SNTE effect within the open perovskite structural class.

ReO_3 has been known as a SNTE material for many years, but there are varying reports of the strength and also extent in temperature over which the effect occurs, which is summarized for recent data by Chatterji[82,115] and Rodriguez[58] in Figure 5 inset. Generally, "open" perovskite oxides are rare due to the requirement of a hexavalent B-site and controlled substitutional studies have not been reported to our knowledge. However, the controlled disorder study by Rodriguez[58] compared crystals synthesized using different growth techniques and clearly showed that the highest quality crystals grown by chemical vapor transport method exhibited the largest and most thermally persistent SNTE effect. As with the physical properties of many perovskite oxides, controlled post-growth annealing procedure studies may be need to be developed to ensure the optimal NTE

effect even in studies of its fundamental causes.

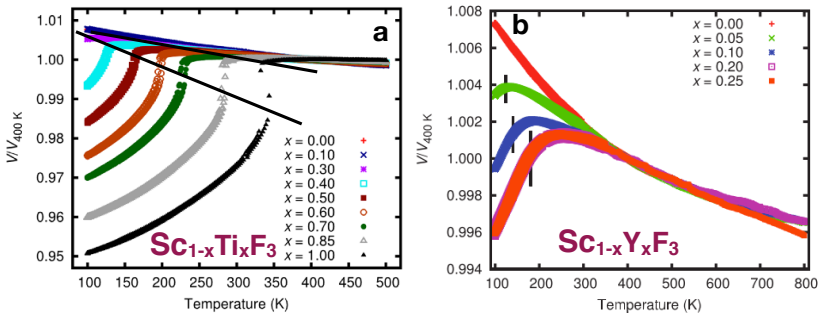

FIG. 8. Compositional dependence of the SNTE effect in $Sc_{1-x}(L = Ti,Y)_xF_3$ for $L = Ti$[94] and $L =Y$[43]. (a) Reprinted with permission from C. R. Morelock et al., Chem. Mater. 26, 1936, (2014). Copyright (2018) American Chemical Society. (b) Reprinted from C. R. Morelock et al. J. Appl. Phys. 114, 213501 (2013), with permission of AIP publishing.

ScF_3 is an unusually clean material - single crystals have been synthesized with 0.002 degree mosaic[116], free of color centers, with high chemical and isotopic purity with readily available components. The flexibility afforded by the trivalent B-site in the trifluorides permits wide chemical tunability and provides new opportunities to observe disorder effects on SNTE. So far, the most thorough and complete studies of the substitutional series $Sc_{1-x}L_xF_3$ have been performed with high inorganic synthesis and high quality structural synchrotron and neutron scattering efforts of the Wilkinson group at Georgia Tech. In a series of papers[43,94,95], substitutions of L=Al,Y,Ti have been reported, particularly the behavior of the cubic-to-rhombohedral phase boundary in this system upon these isovalent substitutions (Figures 8 and 9a). Here we develop a combined analysis of these data which permits conclusions regarding the interaction of disorder and the SNTE effect.

Following the spirit of Attfield, who has studied compositional disorder effects on the A-site of transition metal oxide phase transitions[117–119], we borrow the hypothesis that the ionic radius of the substituted ions represents a local energetic influence on the stability of the ordered phase and discuss in our case the probability distribution $P(r_B)$ of finding a B-site ion of radius r_B in the series $Sc_{1-x}L_xF_3$. We calculate the first two moments of this distribution and associate the mean ionic radius (1st moment) $\langle r_B \rangle$ to an energetic effect on the transition and the variance (2nd moment) σ_B^2 of the distribution as representative of disorder. For the simple binary distributions shown in Figure 9c, these quantities are simply calculated from the nominal composition $M_{1-x}L_xF_3$:

$$\langle r_B \rangle = r_M(1-x) + r_L x \tag{7}$$

$$\sigma_B^2 = x(1-x)(r_L - r_M)^2 \tag{8}$$

$$= (r_M - \langle r_B \rangle)(\langle r_B \rangle - r_L). \tag{9}$$

These relations are general for any binary mixture, and are applied for M=Sc and L=Y,Al,Ti in Figure 9b using the Shannon ionic radius for these trivalent ions. Appropriately, σ_B^2 is zero for the endpoints of the compositional series and is maximum at the 50-50 composition as expected in all cases. Note that for L=Ti, the ion best size matched to Sc, this maximum is small and the effects of disorder are expected to be weaker than for other substitutions, whereas for the much larger Y and much smaller Al ions, disorder increases substantially throughout these series. Further, substitutions of Y have opposite effects on $\langle r_B \rangle$ than substitutions of Ti and Al, therefore the three substitutional series cover well the transition in terms of both energetics and disorder.

Figures 9d,e show the transition temperatures plotted as a function of $\langle r_B \rangle$ and σ_B^2. There is not a clear common trend in either plot, except that the Y and Al substitution series are linear in σ_B^2, implying that quenched disorder is the dominant contribution toward driving the transition, as we have pointed out previously[84]. For the substitution L=Ti, the transition temperature is linear in x, suggesting a dominantly energetic effect, as hypothesized based on its similar size and treated theoretically in the weak-disorder limit of the last section. Figure 9f shows a combined plot of all three series L=Ti,Al,Y as a function of the structural tuning parameter $\langle r_B \rangle$ and the disorder parameter σ_B^2. This generalized disorder-energy analysis unifies the compositional dependencies of three different series with important implications, showing that disorder is deleterious to SNTE and that ScF_3 is situated in a very special place which is difficult to reach in the presence of any disorder. These conclusions and the known variation in the SNTE effect of ReO_3 indicate that disorder generally suppresses the SNTE effect and that careful work optimizing this property with respect to sample history may be necessary in some cases.

ScF_3 has the most dramatic SNTE effect of all members of these series and also appears at a QCP in the diagram of Figure 9f. Figure 8 reproduces the figure panels for thermal expansion in each series and shows that strong SNTE persists above the transition for light substitutional levels, but weakens in all cases. We point out that no known materials exist in the large $\langle r_B \rangle$, small σ_B^2 limit, but if such a composition could be produced, would be of high interest toward exploring the robustness of SNTE to disorder. Furthermore, routine structural refinement experiments performed

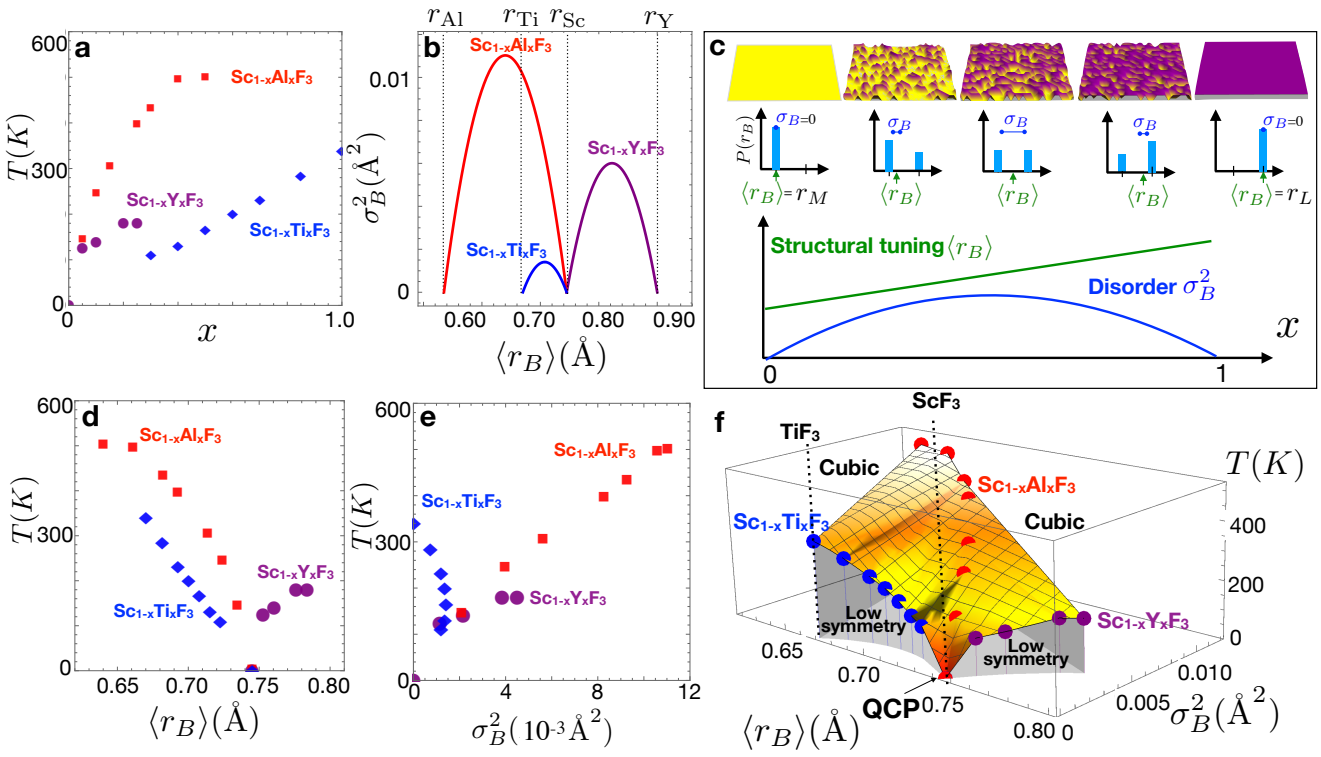

FIG. 9. (a) Cubic-to-rhombohedral transition temperatures T_c(x) in a isovalent substitutional series $Sc_{1-x}L_xF_3$. (b) The dependence of the mean and variance using equation 8 and the Shannon ionic radii of the Ti, Y, and Al. (c, top row) Illustration of the effect of substitution on the potential energy landscape in a solid solution as the composition x is varied. (c, middle row) The binary probability distributions $P(r_B)$ for the five composition levels with the mean and standard deviation σ_B of the distributions indicated by arrows and dumbbells, respectively. (c, bottom) plot of the composition dependence of the first two moments of the distribution according to equations 8. Plot showing the dependence of the transition temperatures as a function of (d) $\langle r_b\rangle$ and (e) σ_B^2, respectively, which show no obvious universal trend. (f) Combined plot of the transition temperatures versus the structural tuning parameter $\langle r_b\rangle$ and the disorder parameter σ_B^2.

at liquid helium temperatures would help immensely toward refining the QCP in these systems where SNTE seems to arise near the T=0 termination of a structural phase boundary.

VI. SUMMARY

We have discussed the broad issue of SNTE with particular focus on perovskite-structured SNTE materials. We have identified the presence of several competing octahedral tilt instabilities occurring near the zero-temperature state of these materials and their associated fluctuations in the high-symmetry phase as key to the SNTE effect in these materials. We have provided a model

treatment beyond mean field theory to account for these fluctuations and identified key elements that move toward control of negative thermal expansion and may be invoked for rational design and discovery of future SNTE systems. We also find that quantum mechanical effects are non-negligible and play an important role in SNTE. Finally, we have described existing data in a new analysis which attempts to isolate the influences of energetics and disorder and presented a holistic and generalizable approach leading to the conclusion that disorder disrupts the balance which drives the SNTE effect in ScF_3, ReO_3, and other SNTE materials. Our thorough combined analysis of the physical properties and special circumstances in this simple structural class has identified trends and influences that we hope will guide discovery of new SNTE materials.

CONFLICT OF INTEREST STATEMENT

The authors declare that the research was conducted in the absence of any commercial or financial relationships that could be construed as a potential conflict of interest.

AUTHOR CONTRIBUTIONS

CAO, SUH and JNH wrote sections 1-3 and 5. GGGV developed the modeling in section 4 and the SM. All authors contributed to writing and revising the manuscript and figures.

FUNDING

Work at the University of Connecticut was provided by National Science Foundation Award No. DMR-1506825 with additional support from the US Department of Energy, Office of Science, Office of Basic Energy Sciences, under Award No. DE-SC0016481. Work at the University of Costa Rica is supported by the Vice-rectory for Research under project no. 816-B7-601, and work at Argonne National Laboratory is supported by the U.S. Department of Energy, Office of Basic Energy Sciences, Material Sciences and Engineering Division under contract no. DE-AC02-06CH11357.

ACKNOWLEDGMENTS

The authors would like to acknowledge valuable conversations with Peter Littlewood, Richard Brierley, Premala Chandra, and Alexander Balatsky. GGGV acknowledges Churchill College, the

Department of Materials Science and Metallurgy and the Cavendish Laboratory at the University of Cambridge where part of this work was done.

---

[1] N. W. Ashcroft and N. David Mermin, *Solid State Physics* (Holt, Rinehart and Winston, 1976).

[2] G D Barrera, J A O Bruno, T H K Barron, and N L Allan, "Negative thermal expansion," Journal of Physics: Condensed Matter **17**, R217–R252 (2005).

[3] W. Miller, C. W. Smith, D. S. Mackenzie, and K. E. Evans, "Negative thermal expansion: a review," Journal of Materials Science **44**, 5441–5451 (2009).

[4] K. Takenaka, T. Hamada, D. Kasugai, and N. Sugimoto, "Tailoring thermal expansion in metal matrix composites blended by antiperovskite manganese nitrides exhibiting giant negative thermal expansion," Journal of Applied Physics **112**, 083517 (2012).

[5] M. Prager and A. Heidemann, "Rotational Tunneling and Neutron Spectroscopy: A Compilation," Chemical Reviews **97**, 2933–2966 (1997).

[6] Jason Hancock, Tim McKnew, Zack Schlesinger, John Sarrao, and Zach Fisk, "Kondo Scaling in the Optical Response of $YbIn_{1-x}Ag_xCu_4$," Physical Review Letters **92**, 186405 (2004).

[7] C E Guillaume, "The Nobel Prize in physics, 1920: Invar alloys," Stockholm, Sweden: Royal Swedish Academy of Sciences , 1–16 (1920).

[8] Masaki Azuma, Wei-tin Chen, Hayato Seki, Michal Czapski, Smirnova Olga, Kengo Oka, Masaichiro Mizumaki, Tetsu Watanuki, Naoki Ishimatsu, Naomi Kawamura, Shintaro Ishiwata, Matthew G Tucker, Yuichi Shimakawa, and J Paul Attfield, "Colossal negative thermal expansion in $BiNiO_3$ induced by intermetallic charge transfer," Nature communications **2**, 347 (2011).

[9] K. Takenaka and H. Takagi, "Giant negative thermal expansion in Ge-doped anti-perovskite manganese nitrides," Applied Physics Letters **87**, 261902 (2005).

[10] BY Qu, HY He, and BC Pan, "Origin of the Giant Negative Thermal Expansion in $Mn_3(Cu_{0.5}Ge_{0.5})N$," Advances in Condensed Matter Physics **2012**, 4903–4906 (2012).

[11] Jun Chen, Longlong Fan, Yang Ren, Zhao Pan, Jinxia Deng, Ranbo Yu, and Xianran Xing, "Unusual Transformation from Strong Negative to Positive Thermal Expansion in $PbTiO_3$-$BiFeO_3$ Perovskite," Physical Review Letters **110**, 115901 (2013).

[12] Jun Chen, Fangfang Wang, Qingzhen Huang, Lei Hu, Xiping Song, Jinxia Deng, Ranbo Yu, and Xianran Xing, "Effectively control negative thermal expansion of single-phase ferroelectrics of $PbTiO_3$-(Bi,La)FeO_3 over a giant range." Scientific reports **3**, 2458 (2013).

[13] Koshi Takenaka, "Progress of Research in Negative Thermal Expansion Materials: Paradigm Shift in the Control of Thermal Expansion," Frontiers in Chemistry **6**, 267 (2018).

[14] T. A. Mary, J. S. O. Evans, T. Vogt, and A. W. Sleight, "Negative Thermal Expansion from 0.3 to 1050 Kelvin in ZrW_2O_8," Science **272**, 90–92 (1996).

[15] JSO Evans, TA Mary, and AW Sleight, "Negative thermal expansion in a large molybdate and tungstate family," Journal of Solid State Chemistry **275**, 61–65 (1997).

[16] JSO Evans, Z Hu, JD Jorgensen, and DN Argyriou, "Compressibility, phase transitions, and oxygen migration in zirconium tungstate, ZrW_2O_8," Science **132**, 15496–15498 (1997).

[17] Alexandra K.A. Pryde, Kenton D. Hammonds, Martin T. Dove, Volker Heine, Julian D. Gale, and Michele C. Warren, "Rigid unit modes and the negative thermal expansion in ZrW_2O_8," Phase Transitions **61**, 141–153 (1997).

[18] CA Perottoni and JAH Da Jornada, "Pressure-induced amorphization and negative thermal expansion in ZrW_2O_8," Science **280**, 886–889 (1998).

[19] A. Ramirez and G. Kowach, "Large Low Temperature Specific Heat in the Negative Thermal Expansion Compound ZrW_2O_8," Physical Review Letters **80**, 4903–4906 (1998).

[20] G Ernst, C Broholm, GR Kowach, and AP Ramirez, "Phonon density of states and negative thermal expansion in ZrW_2O_8," Nature **583**, 580–583 (1998).

[21] A.P Ramirez, C.L Broholm, R.J Cava, and G.R Kowach, "Geometrical frustration, spin ice and negative thermal expansion the physics of underconstraint," Physica B: Condensed Matter **280**, 290–295 (2000).

[22] R. Mittal, S. Chaplot, H. Schober, and T. Mary, "Origin of Negative Thermal Expansion in Cubic ZrW_2O_8 Revealed by High Pressure Inelastic Neutron Scattering," Physical Review Letters **86**, 4692–4695 (2001).

[23] D. Cao, F. Bridges, G. Kowach, and A. Ramirez, "Frustrated Soft Modes and Negative Thermal Expansion in ZrW_2O_8," Physical Review Letters **89**, 215902 (2002).

[24] Lizhi Ouyang, Yong-Nian. Xu, and W. Ching, "Electronic structure of cubic and orthorhombic phases of ZrW_2O_8," Physical Review B **65**, 113110 (2002).

[25] D Cao, F Bridges, GR Kowach, and AP Ramirez, "Correlated atomic motions in the negative thermal expansion material ZrW_2O_8: A local structure study," Physical Review B **79**, 184302 (2003).

[26] F. Drymiotis, H. Ledbetter, J. Betts, T. Kimura, J. Lashley, A. Migliori, A. Ramirez, G. Kowach, and J. Van Duijn, "Monocrystal Elastic Constants of the Negative-Thermal-Expansion Compound Zirconium Tungstate (ZrW_2O_8)," Physical Review Letters **93**, 025502 (2004).

[27] R. Mittal, S. L. Chaplot, H. Schober, A. I. Kolesnikov, C.-K. Loong, C. Lind, and A. P. Wilkinson, "Negative thermal expansion in cubic $ZrMo_2O_8$: Inelastic neutron scattering and lattice dynamical studies," Physical Review B **70**, 214303 (2004).

[28] Jason Hancock, Chandra Turpen, Zack Schlesinger, Glen Kowach, and Arthur Ramirez, "Unusual Low-Energy Phonon Dynamics in the Negative Thermal Expansion Compound ZrW_2O_8," Physical Review Letters **93**, 225501 (2004).

[29] Matthew Tucker, Andrew Goodwin, Martin Dove, David Keen, Stephen Wells, and John Evans, "Negative Thermal Expansion in ZrW_2O_8: Mechanisms, Rigid Unit Modes, and Neutron Total Scattering," Physical Review Letters **95**, 255501 (2005).

[30] CA Kennedy and MA White, "Unusual thermal conductivity of the negative thermal expansion material, ZrW_2O_8," Solid state communications **134**, 271–276 (2005).

[31] C. Pantea, A. Migliori, P. Littlewood, Y. Zhao, H. Ledbetter, J. Lashley, T. Kimura, J. Van Duijn, and G. Kowach, "Pressure-induced elastic softening of monocrystalline zirconium tungstate at 300K," Physical Review B **73**, 214118 (2006).

[32] David Keen, Andrew Goodwin, Matthew Tucker, Martin Dove, John Evans, Wilson Crichton, and Michela Brunelli, "Structural Description of Pressure-Induced Amorphization in ZrW_2O_8," Physical Review Letters **98**, 225501 (2007).

[33] Matthew G Tucker, David A Keen, John S O Evans, and Martin T Dove, "Local structure in ZrW_2O_8 from neutron total scattering," Journal of physics. Condensed matter **19**, 335215 (2007).

[34] C. Figueirêdo and C. Perottoni, "B3LYP density functional calculations on the ground-state structure, elastic properties, and compression mechanism of α-ZrW_2O_8," Physical Review B **75**, 184110 (2007).

[35] Z. Schlesinger, J. A. Rosen, J. N. Hancock, and A. P. Ramirez, "Soft Manifold Dynamics behind Negative Thermal Expansion," Physical Review Letters **101**, 015501 (2008).

[36] David A. Keen, Andrew L. Goodwin, Matthew G. Tucker, Joseph A. Hriljac, Thomas D. Bennett, Martin T. Dove, Annette K. Kleppe, Andrew P. Jephcoat, and Michela Brunelli, "Diffraction study of pressure-amorphized ZrW_2O_8 using in situ and recovered samples," Physical Review B **83**, 064109 (2011).

[37] Leighanne C Gallington, Karena W Chapman, Cody R Morelock, Peter J Chupas, and Angus P Wilkinson, "Orientational order-dependent thermal expansion and compressibility of ZrW_2O_8 and $ZrMo_2O_8$," Physical chemistry chemical physics : PCCP **15**, 19665–72 (2013).

[38] M. K. Gupta, R. Mittal, and S. L. Chaplot, "Negative thermal expansion in cubic ZrW_2O_8: Role of phonons in the entire Brillouin zone from ab initio calculations," Physical Review B **88**, 014303 (2013).

[39] Leighanne C. Gallington, Karena W. Chapman, Cody R. Morelock, Peter J. Chupas, and Angus P. Wilkinson, "Dramatic softening of the negative thermal expansion material HfW_2O_8 upon heating through its WO_4 orientational order-disorder phase transition," Journal of Applied Physics **115**, 053512 (2014).

[40] F. Bridges, T. Keiber, P. Juhas, S. J. L. Billinge, L. Sutton, J. Wilde, and Glen R. Kowach, "Local Vibrations and Negative Thermal Expansion in ZrW_2O_8," Physical Review Letters **112**, 045505 (2014).

[41] Andrea Sanson, "Toward an Understanding of the Local Origin of Negative Thermal Expansion in ZrW_2O_8: Limits and Inconsistencies of the Tent and Rigid Unit Mode Models," Chemistry of Materials **26**, 3716–3720 (2014).

[42] Benjamin K Greve, Kenneth L Martin, Peter L Lee, Peter J Chupas, Karena W Chapman, and Angus P Wilkinson, "Pronounced negative thermal expansion from a simple structure: cubic ScF_3," Journal of the American Chemical Society **132**, 15496–8 (2010).

[43] Cody R. Morelock, Benjamin K. Greve, Leighanne C. Gallington, Karena W. Chapman, and Angus P. Wilkinson, "Negative thermal expansion and compressibility of $Sc_{1-x}Y_xF_3$ ($x \leq 0.25$)," Journal of Applied Physics **114**, 213501 (2013).

[44] Charles Martinek and F. A. Hummel, "Linear Thermal Expansion of Three Tungstates," Journal of the American Ceramic Society **51**, 227–228 (1968).

[45] W. Zhou, H. Wu, T. Yildirim, J. Simpson, and A. Walker, "Origin of the exceptional negative thermal expansion in metal-organic framework-5 Zn_4O(1,4-benzenedicarboxylate)$_3$," Physical Review B **78**, 054114 (2008).

[46] Sang Soo Han and William A. Goddard, "Metal–Organic Frameworks Provide Large Negative Thermal Expansion Behavior," The Journal of Physical Chemistry C **111**, 15185–15191 (2007).

[47] Kwanghee Lee, Reghu Menon, C. Yoon, and A. Heeger, "Direct observation of a transverse vibrational mechanism for negative thermal expansion in $Zn(CN)_2$: an atomic pair distribution function analysis." Journal of the American Chemical Society **127**, 15630–6 (2005).

[48] R. Mittal, M.K. Gupta, and S.L. Chaplot, "Phonons and anomalous thermal expansion behaviour in crystalline solids," Progress in Materials Science **92**, 360–445 (2018).

[49] Glen R. Kowach and A. P. Ramirez, *Handbook of Materials Selection* (John Wiley & Sons, Inc., New York, 2002).

[50] D.A. Fleming, D.W. Johnson, and P.J. Lemaire, "A Temperature Compensated Optical Fiber Refractive Index Grating," (1997).

[51] Dorian K. Balch and David C. Dunand, "Copper-zirconium tungstate composites exhibiting low and negative thermal expansion influenced by reinforcement phase transformations," Metallurgical and Materials Transactions A **35**, 1159–1165 (2004).

[52] Klaartje De Buysser, Petra Lommens, Christy De Meyer, Els Bruneel, Serge Hoste, and Isabel Van Driessche, "ZrO_2-ZrW_2O_8 composites with tailor-made thermal expansion," Ceramics-Silikaty **48**, 139–144 (2004).

[53] P. Lommens, C. De Meyer, E. Bruneel, K. De Buysser, I. Van Driessche, and S. Hoste, "Synthesis and thermal expansion of ZrO_2/ZrW_2O_8 composites," Journal of the European Ceramic Society **25**, 3605–3610 (2005).

[54] Lisa M. Sullivan and Charles M. Lukehart, "Zirconium Tungstate (ZrW_2O_8)/Polyimide Nanocomposites Exhibiting Reduced Coefficient of Thermal Expansion," Chemistry of Materials **17**, 2136–2141 (2005).

[55] Cora Lind, Maria R. Coleman, Leah C. Kozy, and Gayathri R. Sharma, "Zirconium tungstate/polymer nanocomposites: Challenges and opportunities," Physica Status Solidi B **248**, 123–129 (2011).

[56] T R Ravindran, Akhilesh K Arora, and T A Mary, "High-pressure Raman spectroscopic study of zirconium tungstate," Journal of Physics-Condensed Matter **13**, 11573–11588 (2001).

[57] Martin T Dove and Hong Fang, "Negative thermal expansion and associated anomalous physical properties: review of the lattice dynamics theoretical foundation," Reports on Progress in Physics **79**, 066503 (2016).

[58] Efrain E. Rodriguez, Anna Llobet, Thomas Proffen, Brent C. Melot, Ram Seshadri, Peter B. Littlewood, and Anthony K. Cheetham, "The role of static disorder in negative thermal expansion in ReO_3," Journal of Applied Physics **105**, 114901 (2009).

[59] Justin C. Hancock, Karena W. Chapman, Gregory J. Halder, Cody R. Morelock, Benjamin S. Kaplan, Leighanne C. Gallington, Angelo Bongiorno, Chu Han, Si Zhou, and Angus P. Wilkinson, "Large Negative Thermal Expansion and Anomalous Behavior on Compression in Cubic ReO_3 - Type $A^{II}B^{IV}F_6$: $CaZrF_6$ and $CaHfF_6$," Chemistry of Materials **27**, 3912–3918 (2015).

[60] T. Kimura, S. Ishihara, H. Shintani, T. Arima, K. T. Takahashi, K. Ishizaka, and Y. Tokura, "Distorted Perovskite with e_g^1 Configuration as a Frustrated Spin System," Physical Review B **68**, 060403 (2002), arXiv:0211568 [cond-mat].

[61] S. Maekawa, T. Tohyama, S.E. Barnes, S. Ishihara, W. Koshibae, and G. Khaliullin, eds., *Physics of Transition Metal Oxides* (Springer-Verlag, 2004).

[62] Shigeyuki Takagi, Alaska Subedi, David J. Singh, and Valentino R. Cooper, "Polar behavior of the double perovskites BiMZnNbO_6 (M = Pb and Sr) from density-functional calculations," Physical Review B **81**, 134106 (2010).

[63] J.H. Ngai, F.J. Walker, and C.H. Ahn, "Correlated oxide physics and electronics," Annual Review of Materials Research **44**, 1–17 (2014).

[64] A. M. Glazer, "The classification of tilted octahedra in perovskites," Acta Crystallographica Section B Structural Crystallography and Crystal Chemistry **28**, 3384–3392 (1972).

[65] A. M. Glazer and IUCr, "Simple ways of determining perovskite structures," Acta Crystallographica Section A **31**, 756–762 (1975).

[66] Nicole A. Benedek and Craig J. Fennie, "Why Are There So Few Perovskite Ferroelectrics?" The Journal of Physical Chemistry C **117**, 13339–13349 (2013).

[67] Hiromi Unoki and Tunetaro Sakudo, "Electron Spin Resonance of Fe^{3+} in $SrTiO_3$ with Special Reference to the 110K Phase Transition," Journal of the Physical Society of Japan **23**, 546–552 (1967).

[68] R. A. Cowley, W. J.L. Buyers, and G. Dolling, "Relationship of normal modes of vibration of strontium titanate and its antiferroelectric phase transition at 110K," Solid State Communications **7**, 181–184 (1969).

[69] R. A. Cowley, "Lattice Dynamics and Phase Transitions of Strontium Titanate," Physical Review **134** (1964), 10.1103/PhysRev.134.A981.

[70] G. Shirane and Y. Yamada, "Lattice-dynamical study of the 110K phase transition in $SrTiO_3$," Physical Review **177**, 858–863 (1969).

[71] P. A. Fleury, J. F. Scott, and J. M. Worlock, "Soft phonon modes and the 110K phase transition in $SrTiO_3$," Physical Review Letters **21**, 16–19 (1968), arXiv:arXiv:1011.1669v3.

[72] R. O. Bell and G. Rupprecht, "Elastic constants of strontium titanate," Physical Review **129**, 90–94 (1963).

[73] G. Shirane, "Neutron scattering studies of structural phase transitions at Brookhaven," Reviews of Modern Physics **46**, 437–449 (1974).

[74] R.A. Cowley, "Structural phase transitions I. Landau theory," Advances in Physics **29**, 1–110 (1980).

[75] J. F. Scott, "Soft-mode spectroscopy: Experimental studies of structural phase transitions," Reviews of Modern Physics **46**, 83–128 (1974).

[76] B. Halperin and C. Varma, "Defects and the central peak near structural phase transitions," Physical Review B **14**, 4030–4044 (1976).

[77] J Topler, B Alefeld, and A Heidemann, "Study of the central peak of $SrTiO_3$ by neutron spectroscopy with high energy resolution," Journal of Physics C: Solid State Physics **10**, 635–643 (1977).

[78] T. Riste, E. J. Samuelsen, K. Otnes, and J. Feder, "Critical behaviour of $SrTiO_3$ near the 105K phase transition," Solid State Communications **88**, 901–904 (1993).

[79] Subir Sachdev and Bernhard Keimer, "Quantum criticality," Physics Today **64**, 29–35 (2011), arXiv:1102.4628.

[80] Piers Coleman and Andrew J Schofield, "Quantum criticality," Nature **433**, 226–229 (2005).

[81] Philipp Gegenwart, Qimiao Si, and Frank Steglich, "Quantum criticality in heavy-fermion metals," Nature Physics **4**, 186–197 (2008).

[82] Tapan Chatterji, Thomas C. Hansen, Michela Brunelli, and Paul F. Henry, "Negative thermal expansion of ReO_3 in the extended temperature range," Applied Physics Letters **94**, 241902 (2009).

[83] Monica Dapiaggi and Andy N. Fitch, "Negative (and very low) thermal expansion in ReO_3 from 5 to 300 K," Journal of Applied Crystallography **42**, 253–258 (2009).

[84] Sahan U. Handunkanda, Erin B. Curry, Vladimir Voronov, Ayman H. Said, Gian G. Guzmán-Verri, Richard T. Brierley, Peter B. Littlewood, and Jason N. Hancock, "Large isotropic negative thermal expansion above a structural quantum phase transition," Physical Review B **92**, 134101 (2015).

[85] J. D. Axe, Y. Fujii, B. Batlogg, M. Greenblatt, and S. Di Gregorio, "Neutron scattering study of the pressure-induced phase transformation in ReO_3," Physical Review B **31**, 663–667 (1985).

[86] J. E. Schirber and B. Morosin, ""Compressibility Collapse" Transition in ReO_3," Physical Review Letters **42**, 1485–1487 (1979).

[87] J.-E. Jørgensen, J. Jorgensen, B. Batlogg, J. Remeika, and J. Axe, "Order parameter and critical exponent for the pressure-induced phase transitions in ReO_3," Physical Review B **33**, 4793–4798 (1986).

[88] J.-E. Jørgensen, W. G. Marshall, R. I. Smith, J. Staun Olsen, and L. Gerward, "High-pressure neutron powder diffraction study of the $Im\bar{3}$ phase of ReO_3," Journal of Applied Crystallography **37**, 857–861 (2004).

[89] Tapan Chatterji, P. Freeman, M. Jimenez-Ruiz, R. Mittal, and S. Chaplot, "Pressure- and temperature-induced M_3 phonon softening in ReO_3," Physical Review B **79**, 184302 (2009).

[90] Carl P. Romao, Cody R. Morelock, Michel B. Johnson, J. W. Zwanziger, Angus P. Wilkinson, and Mary Anne White, "The heat capacities of thermomiotic ScF_3 and ScF_3YF_3 solid solutions," Journal of Materials Science **50**, 3409–3415 (2015).

[91] K. S. Aleksandrov, V. N. Voronov, A. N. Vtyurin, A. S. Krylov, M. S. Molokeev, M. S. Pavlovski, S. V. Goryanov, A. Yu. Likhacheva, and A. I. Ancharov, "Pressure-induced phase transition in the cubic ScF_3 crystal," Physics of the Solid State **51**, 810–816 (2009).

[92] K. S. Aleksandrov, N. V. Voronov, A. N. Vtyurin, A. S. Krylov, M. S. Molokeev, A. S. Oreshonkov, S. V. Goryainov, A. Yu. Likhacheva, and A. I. Ancharov, "Structure and lattice dynamics of the high-pressure

phase in the ScF_3 crystal," Physics of the Solid State **53**, 564–569 (2011).

[93] Cody R. Morelock, Benjamin K. Greve, Mehmet Cetinkol, Karena W. Chapman, Peter J. Chupas, and Angus P. Wilkinson, "Role of Anion Site Disorder in the Near Zero Thermal Expansion of Tantalum Oxyfluoride," Chemistry of Materials **25**, 1900–1904 (2013).

[94] C. R. Morelock, L. C. Gallington, and A. P. Wilkinson, "Evolution of negative thermal expansion and phase transitions in $Sc_{1-x}Ti_xF_3$," Chem. Mater. **26**, 1936 (2014).

[95] C. R. Morelock, L. C. Gallington, and A. P. Wilkinson, "Solid solubility, phase transitions, thermal expansion, and compressibility in $Sc_{1-x}Al_xF_3$," J. Solid State Chem. **222**, 96 (2015).

[96] K. S. Aleksandrov, V. N. Voronov, A. N. Vtyurin, S. A. Goryainov, N. G. Zamkova, V. I. Zinenko, and A. S. Krylov, "Pressure-Induced Phase Transitions in ScF_3 Crystal–Raman Spectra and Lattice Dynamics," Ferroelectrics **284**, 31–45 (2003).

[97] M K Gupta, Baltej Singh, R Mittal, and S L Chaplot, "Negative Thermal Expansion Behaviour in $MZrF_6$ (M = Ca, Mg, Sr): Ab-initio Lattice Dynamical Studies," arXiv (2018).

[98] Connor A Occhialini, Sahan U Handunkanda, Ayman Said, Sudhir Trivedi, G G Guzmán-Verri, and Jason N Hancock, "Negative thermal expansion near two structural quantum phase transitions," Physical Review Materials **1**, 070603(R) (2017).

[99] Andrew L Goodwin, Mark Calleja, Michael J Conterio, Martin T Dove, John S O Evans, David A Keen, Lars Peters, and Matthew G Tucker, "Colossal positive and negative thermal expansion in the framework material $Ag_3[Co(CN)_6]$," Science **319**, 794–7 (2008).

[100] Vanessa E. Fairbank, Amber L. Thompson, Richard I. Cooper, and Andrew L. Goodwin, "Charge-ice dynamics in the negative thermal expansion material $Cd(CN)_2$," Physical Review B **86**, 104113 (2012).

[101] R. Mittal, S. L. Chaplot, and H. Schober, "Measurement of anharmonicity of phonons in the negative thermal expansion compound $Zn(CN)_2$ by high pressure inelastic neutron scattering," Applied Physics Letters **95**, 201901 (2009).

[102] A.P. Giddy, M.T. Dove, G.S. Pawley, and V. Heine, "The determination of rigid-unit modes as potential soft modes for displacive phase transitions in framework crystal structures," Acta Crystallographica Section A: Foundations of Crystallography **49** (1993), 10.1107/S0108767393002545.

[103] A. Corrales-Salazar, R. T. Brierley, P. B. Littlewood, and G. G. Guzmán-Verri, "Landau theory and giant room-temperature barocaloric effect in MF_3 metal trifluorides," Physical Review Materials **1**, 053601 (2017).

[104] Y.-R. Chen, V. Perebeinos, and P. B. Allen, "Density-functional study of the cubic-to-rhombohedral transition in α-AlF_3," Physical Review B **69**, 054109 (2004).

[105] S. Chaudhuri, P. J. Chupas, M. Wilson, P. Madden, and C. P. Grey, "Study of the nature and mechanism of the rhombohedral-to-cubic phase transition in α-AlF_3 with molecular dynamics simulations," J. Phys. Chem. B **108**, 3437 (2004).

[106] P. Allen, Y.-R. Chen, S. Chaudhuri, and C. Grey, "Octahedral tilt instability of ReO_3-type crystals," Physical Review B **73**, 172102 (2006).

[107] H. Volker, P. R. L. Welche, and M. T. Dove, "Geometrical origin and theory of negative thermal expansion in framework structures," Journal of the American Ceramic Society **82**, 1793 (2004).

[108] J. Feder and E. Pytte, "Theory of a structural phase transition in perovskite-type crystals. ii. interaction with elastic strain," Physical Review B **1**, 4803–4810 (1970).

[109] P. Daniel, A. Bulou, M. Rousseau, J. Nouet, J. L. Fourquet, M. Leblanc, and R. Burriel, "A study of the structural phase transitions in AlF_3: x-ray powder diffraction, differential scanning calorimetry (DSC) and Raman scattering investigations of the lattice dynamics and phonon spectrum," J. Phys. Condens. Matter **2**, 5663 (1990).

[110] Chen W. Li, Xiaoli Tang, J. A. Muñoz, J. B. Keith, S. J. Tracy, D. L. Abernathy, and B. Fultz, "Structural Relationship between Negative Thermal Expansion and Quartic Anharmonicity of Cubic ScF_3," Physical Review Letters **107**, 195504 (2011).

[111] K. Rabe, C.H. Ahn, and J.-M. Triscone, eds., *Physics of Ferroelectrics: A modern perspective* (Springer-Verlag, Berlin, 2007).

[112] E. Pytte, "Theory of perovskite ferroelectrics," Physical Review B **5**, 3758–3769 (1972).

[113] A. van Roekeghem, J. Carrete, and N. Mingo, "Anomalous thermal conductivity and suppression of negative thermal expansion in ScF_3," Physical Review B **94**, 020303 (2016).

[114] Yaming Liu, Zhenhong Wang, Mingyi Wu, Qiang Sun, Mingju Chao, and Yu Jia, "Negative thermal expansion in isostructural cubic ReO_3 and ScF_3: A comparative study," Computational Materials Science **107**, 157–162 (2015).

[115] Tapan Chatterji and G.J. McIntyre, "Pressure-induced structural phase transition in ReO3," Solid State Communications **139**, 12–15 (2006).

[116] Sahan U. Handunkanda, Connor A. Occhialini, Ayman H. Said, and Jason N. Hancock, "Two-dimensional nanoscale correlations in the strong negative thermal expansion material ScF_3," Physical Review B **94**, 214102 (2016).

[117] J. Paul Attfield, "A Simple Approach to Lattice Effects in Conducting Perovskite-Type Oxides," Chemistry of Materials **10**, 3239–3248 (1998).

[118] J.P Attfield, "Structureproperty relations in doped perovskite oxides," International Journal of Inorganic Materials **3**, 1147–1152 (2001).

[119] J.P. Attfield, "A' cation control of perovskite properties," Crystal Engineering **5**, 427–438 (2002).

Supplmentary Material: Negative thermal expansion in open perovskites near the precipice of structural stability

I. MODEL HAMILTONIAN

We consider a cubic lattice with N sites and choose normal mode coordinates that describe local displacements $\boldsymbol{Q}_i = (Q_{ix}, Q_{iy}, Q_{iz})$ in the unit cell $i\,(i = 1, 2, ..., N)$ that are associated with the relevant soft R_4^+ phonon mode, the condensation of which leads to a structural transition to a rhombohedral $R\overline{3}c$ phase. In addition, we introduce symmetry adapted strains $\epsilon_{ia} = \epsilon_{i1} + \epsilon_{i2} + \epsilon_{i3}, \epsilon_{it} = (2\epsilon_{i3} - \epsilon_{i2} - \epsilon_{i1})/\sqrt{3}$ and $\epsilon_{io} = \epsilon_{i1} - \epsilon_{i2}$, as well as shear strain components $\epsilon_{i4}, \epsilon_{i5}$, and ϵ_{i6} in the usual Voigt notation: $\epsilon_{i\alpha} = \partial u_{i\alpha}/\partial x_\alpha$ $(\alpha = 1, 2, 3)$, $\epsilon_{i4} = 2\left(\partial u_{iy}/\partial z + \partial u_{iz}/\partial y\right), \epsilon_{i5} = 2\left(\partial u_{ix}/\partial z + \partial u_{iz}/\partial x\right)$, and $\epsilon_{i6} = 2\left(\partial u_{ix}/\partial y + \partial u_{iy}/\partial x\right)$. $\boldsymbol{u}_i = (u_{ix}, u_{iy}, u_{iz})$ is the displacement of the center of mass of the unit cell i from its equilibrium position due to the acoustic phonon mode. Physically, ϵ_{ia} and $\epsilon_{it/o}$ are, respectively, volume and tetragonal strains. We consider the model Hamiltonian,

$$H = H_Q + H_\epsilon + H_{Q\epsilon}, \tag{S1}$$

where,

$$H_Q = \frac{1}{2}\sum_{i,\lambda}\Pi_{i\nu}^2 + \frac{1}{2}\sum_{i,\lambda}\kappa_i Q_{i\nu}^2 + \frac{\gamma_1}{4}\sum_{i,\lambda\lambda'}Q_{i\lambda}^2 Q_{i\lambda'}^2 + \frac{\gamma_2}{2}\sum_{i,\lambda\neq\lambda'}Q_{i\nu}^2 Q_{i\nu'}^2 - \frac{1}{2}\sum_{ij,\lambda\lambda'}Q_{i\lambda}v_{ij}^{\lambda\lambda'}Q_{j\lambda'}, \tag{S2}$$

$$H_\epsilon = \frac{1}{2}\sum_i |\boldsymbol{\pi}_i|^2 + \frac{1}{2}\sum_i \left[C_a\epsilon_{ia}^2 + C_t\left(\epsilon_{it}^2 + \epsilon_{io}^2\right) + C_r\left(\epsilon_{i4}^2 + \epsilon_{i5}^2 + \epsilon_{i6}^2\right)\right] + P\sum_i \epsilon_{ia}, \tag{S3}$$

and

$$\begin{aligned} H_{Q\epsilon} = {} & g_a\sum_i \epsilon_{ia}\left|\boldsymbol{Q}_i\right|^2 - g_t\sum_i\left[\left(Q_{ix}^2 - Q_{iy}^2\right)\epsilon_{io} + \frac{1}{\sqrt{3}}\left(2Q_{iz}^2 - Q_{iy}^2 - Q_{ix}^2\right)\epsilon_{it}\right] \\ & - g_r\sum_i\left(Q_{ix}Q_{iy}\epsilon_{i6} + Q_{ix}Q_{iz}\epsilon_{i5} + Q_{iy}Q_{iz}\epsilon_{i4}\right). \end{aligned} \tag{S4}$$

Here, $\boldsymbol{\Pi}_i$ and $\boldsymbol{\pi}_i$ are, respectively, the conjugate momenta of $\boldsymbol{Q}_i$ and $\boldsymbol{u}_i$. $\boldsymbol{v}_{ij}^{\lambda\lambda'}$ $(\lambda, \lambda' = x, y, z)$ is an interaction between the soft mode coordinates with Fourier transform $\boldsymbol{v}_{\boldsymbol{R}+\boldsymbol{q}}^{\lambda\lambda'} = v_{\boldsymbol{R}}\delta_{\lambda\lambda'} + q^2 F_{\lambda\lambda'}\left(\hat{\boldsymbol{q}}\right)$. This form is typical of cubic lattices with $F_{\lambda\lambda'}\left(\hat{\boldsymbol{q}}\right)$ dependent on the direction of the unit wave-vector $\hat{\boldsymbol{q}} = \boldsymbol{q}/q$ and independent of the magnitude q.[R1] Within the local SCPA, the equations

derived from the stationary property of the free energy are independent of the particular form of $F_{\lambda\lambda'}(\hat{\boldsymbol{q}})$ as long as there is no self-interaction.[R2] $C_a = (C_{11} + 2C_{12})/3$, is the bulk modulus, and $C_t = (C_{11} - C_{12})/2, C_r = C_{44}$, are deviatoric and shear moduli, respectively. g_a, g_t, and g_r are coupling constants between the lattice and the strain degrees of freedom, and P is an applied hydrostatic pressure. κ_i is the lattice stiffness at site i; γ_1 and γ_2 are coefficients of the isotropic and anisotropic cubic anharmonicites, respectively.

To account for quenched compositional disorder in mixed-compounds, we note that at the mean field level the energy barriers between different lattice stuctures depend on the ratio between the harmonic and anharmonic coefficients of the model.[R1] For simplicity, we thus consider a probability distribution $\mathcal{P}(\kappa_1, \kappa_2, ..., \kappa_N)$ for the κ's while assuming that the remaining parameters remain fixed.

To solve the statistical mechanical problem posed by the Hamiltonian (S1), we use a variational formulation of a SCPA in which the energies of the phonon excitations, displacement and strain order parameters are determined from the minimization of the free energy.[R2]

II. STATISTICAL MECHANICAL SOLUTION

We consider the trial probability distribution,

$$\rho^{tr} = \frac{e^{-\beta H^{tr}}}{Z^{tr}}, \tag{S5}$$

where H^{tr} is the Hamiltonian of the local uncoupled problem,

$$H^{tr} = H_Q^{tr} + H_\epsilon^{tr}, \tag{S6}$$

$$H_Q^{tr} = \frac{1}{2}\sum_i |\boldsymbol{\Pi}_i|^2 + \frac{1}{2}\sum_{i,\alpha\beta} (Q_{i\alpha} - A_{i\alpha})\, \mathcal{M}_{\alpha\beta}\, (Q_{i\beta} - A_{i\beta}), \tag{S7}$$

$$H_\epsilon^{tr} = \frac{1}{2}\sum_i |\boldsymbol{\pi}_i|^2 + \frac{1}{2}\sum_{i,\alpha\beta} (\epsilon_{i\alpha} - e_{i\alpha})\, C_{\alpha\beta}\, (\epsilon_{i\beta} - e_{i\beta}). \tag{S8}$$

$Z^{tr} = \mathrm{Tr} e^{-\beta H^{tr}}$ is its normalization. $A_{i\alpha} = \langle Q_{i\alpha} \rangle$ and $e_{i\alpha} = \langle e_{i\alpha} \rangle$ are the spontaneous displacement and strain order parameters which will be determined by minimization of the free energy; $\mathcal{M}_{\alpha\beta}$ is the dynamical matrix with eigenfrequencies ω_λ of the non-ineracting problem ($v_{ij}^{\lambda\lambda'} = 0$). Here, $\langle ... \rangle = \mathrm{Tr}\left\{\rho^{tr} ....\right\}$ denotes thermal average over the trial probability distribution (S5). We set the long-range ordering associated with the condenstation of the R_4^+ mode at $R = (1,1,1)(\pi/a)$, by writing $A_{i\alpha} = A_\alpha e^{i\boldsymbol{R}\cdot\boldsymbol{r}_i}$, where $\boldsymbol{r}_i$ is the position vector the lattice site i. This corresponds to out-of-phase tilts where $A_{i\lambda}$ changes sign from site to site.

A. Free energy

The free energy is calculated in the usual way $F = \langle H \rangle + k_B T \left\langle \ln \rho^{tr} \right\rangle$,

$$F = F_Q + F_\epsilon + F_{Q\epsilon}, \tag{S9}$$

where,

$$\frac{F_Q}{N} = \frac{\overline{\kappa}}{2} \langle\, |\boldsymbol{Q}|^2 \,\rangle + \frac{\gamma_1}{4} \langle\, |\boldsymbol{Q}|^4 \,\rangle + \frac{\gamma_2}{2} \left(\left\langle Q_x^2 Q_y^2 \right\rangle + \left\langle Q_x^2 Q_z^2 \right\rangle + \left\langle Q_y^2 Q_z^2 \right\rangle \right) - \frac{1}{2} \sum_{\lambda\lambda'} v_R^{\lambda\lambda'} \langle Q_\lambda \rangle \langle Q_{\lambda'} \rangle$$
$$- k_B T \sum_\lambda \left\{ \frac{\beta\omega_\lambda}{2} \coth\left(\frac{\beta\omega_\lambda}{2} \right) - \ln\left[2 \sinh\left(\frac{\beta\omega_\lambda}{2} \right) \right] \right\}, \tag{S10}$$

$$\frac{F_\epsilon}{N} = \frac{1}{2} \left[C_a e_a^2 + C_t \left(e_t^2 + e_o^2 \right) + C_r \sum_{\nu=4}^{6} e_\nu^2 \right] + P e_a, \tag{S11}$$

and,

$$\frac{F_{Q\epsilon}}{N} = g_a e_a \langle\, |\boldsymbol{Q}|^2 \,\rangle - g_t \left[\left(\left\langle Q_x^2 \right\rangle - \left\langle Q_y^2 \right\rangle \right) e_o + \frac{1}{\sqrt{3}} \left(2 \left\langle Q_z^2 \right\rangle - \left\langle Q_x^2 \right\rangle - \left\langle Q_x^2 \right\rangle \right) e_t \right]$$
$$- g_r \left[\langle Q_x Q_y \rangle e_6 + \langle Q_x Q_z \rangle e_5 + \langle Q_y Q_z \rangle e_4 \right], \tag{S12}$$

with

$$\langle Q_\lambda Q_{\lambda'} \rangle = A_\lambda A_{\lambda'} + \psi_{\lambda\lambda'}, \tag{S13a}$$
$$\left\langle Q_\lambda^2 Q_{\lambda'}^2 \right\rangle = A_\lambda^2 A_{\lambda'}^2 + A_\lambda^2 \psi_{\lambda'\lambda'} + 4 A_\lambda A_{\lambda'} \psi_{\lambda\lambda'} + A_{\lambda'}^2 \psi_{\lambda\lambda} + \psi_{\lambda\lambda} \psi_{\lambda'\lambda'} + 2\psi_{\lambda\lambda'}^2. \tag{S13b}$$

$\psi_{\lambda\lambda'}$ are the local OP fluctuations given as follows,

$$\psi_{\lambda\lambda'} = \sum_\nu b_{\lambda\nu}^\dagger b_{\nu\lambda'} \left(\frac{1}{2\omega_\nu} \coth\left(\frac{\beta\omega_\nu}{2} \right) \right), \tag{S14}$$

where $b_{\nu\lambda'}$ is an unitary transformation that diagonalizes $\mathcal{M}_{\alpha\beta}$. $\overline{\kappa}$ the lattice stiffness averaged over compositional disorder. In writing Eq. (S9), we have ignored all terms that do not depend on A_λ, e_α, and ω_λ as they do not have an effect on the miminization procedure.

Minimization of the free energy (S9) with respect to the strains e_α gives the following result,

$$e_a = -\frac{g_a}{C_a} \langle\, |\boldsymbol{Q}|^2 \,\rangle - \frac{P}{C_a}, \tag{S15a}$$
$$e_t = \frac{g_t}{\sqrt{3} C_t} \left(2 \left\langle Q_z^2 \right\rangle - \left\langle Q_x^2 \right\rangle - \left\langle Q_y^2 \right\rangle \right), \tag{S15b}$$
$$e_o = \frac{g_t}{C_t} \left(\left\langle Q_x^2 \right\rangle - \left\langle Q_y^2 \right\rangle \right), \tag{S15c}$$
$$e_4 = \frac{g_r}{C_r} \langle Q_y Q_z \rangle, \quad e_5 = \frac{g_r}{C_r} \langle Q_x Q_z \rangle, \quad e_6 = \frac{g_r}{C_r} \langle Q_x Q_y \rangle. \tag{S15d}$$

By substituting the strains of Eq. (S15) into the Eq. (S9), we obtain a free energy which depends on the displacements $\boldsymbol{Q}$ only, where,

$$\begin{aligned}\frac{\tilde{F}}{N} &= \frac{\tilde{\kappa}}{2}\left\langle\, |\boldsymbol{Q}|^2 \,\right\rangle + \frac{\gamma_1}{4}\left\langle\, |\boldsymbol{Q}|^4 \,\right\rangle + \frac{\gamma_2}{2}\left(\left\langle Q_x^2 Q_y^2\right\rangle + \left\langle Q_x^2 Q_z^2\right\rangle + \left\langle Q_y^2 Q_z^2\right\rangle\right) - \frac{1}{2}\sum_{\lambda\lambda'} v_R^{\lambda\lambda'}\left\langle Q_\lambda Q_{\lambda'}\right\rangle, \\ &- k_B T \sum_\lambda \left\{ \frac{\beta\omega_\lambda}{2}\coth\left(\frac{\beta\omega_\lambda}{2}\right) - \ln\left[2\sinh\left(\frac{\beta\omega_\lambda}{2}\right)\right]\right\}, \\ &- \left(\frac{3}{2}\frac{g_a^2}{C_a} + \frac{2}{3}\frac{g_t^2}{C_t}\right)\left(\left\langle Q_x^2\right\rangle + \left\langle Q_y^2\right\rangle + \left\langle Q_z^2\right\rangle\right)^2 \\ &+ \frac{2g_t^2}{C_t}\left(\left\langle Q_x^2\right\rangle\left\langle Q_y^2\right\rangle + \left\langle Q_x^2\right\rangle\left\langle Q_z^2\right\rangle + \left\langle Q_y^2\right\rangle\left\langle Q_z^2\right\rangle\right) \\ &- \frac{1}{2}\frac{g_r^2}{C_r}\left(\left\langle Q_x Q_y\right\rangle^2 + \left\langle Q_x Q_z\right\rangle^2 + \left\langle Q_y Q_z\right\rangle^2\right) - \frac{P^2}{2C_a}, \end{aligned} \tag{S16}$$

where $\tilde{\kappa} \equiv \overline{\kappa} - 2g_a P/C_a$. The free energies (S9) & (S16) are the starting point for our calculation of the thermodynamic quantities of interest.

B. Soft Mode Frequencies

The soft mode frequencies are computed from the free energy (S9) with the e_α constant and then must be evaluated at the equilibrium points given in Eq (S15). This is because the frequency of the acoustic modes associated with uniform strains vanishes in the long-wavelength limit.[R3]

The dynamical matrix $\mathcal{D}_{\lambda\lambda'}$ of the interacting problem is calculated from the free energy (S9),

$$\begin{aligned}
\mathcal{D}_{xx} &= \frac{\partial^2 \langle H \rangle}{\partial A_x \partial A_x} = \kappa + (2\gamma_1 - \gamma_2)\left\langle Q_x^2 \right\rangle + (\gamma_1 + \gamma_2)\left\langle \, |\boldsymbol{Q}|^2 \, \right\rangle \\
&\qquad + 2g_a e_a - 2g_t\left(e_o - \frac{e_t}{\sqrt{3}}\right) - v_R, \\
\mathcal{D}_{yy} &= \frac{\partial^2 \langle H \rangle}{\partial A_y \partial A_y} = \kappa + (2\gamma_1 - \gamma_2)\left\langle Q_y^2 \right\rangle + (\gamma_1 + \gamma_2)\left\langle \, |\boldsymbol{Q}|^2 \, \right\rangle \\
&\qquad + 2g_a e_a + 2g_t\left(e_o + \frac{e_t}{\sqrt{3}}\right) - v_R, \\
\mathcal{D}_{zy} &= \frac{\partial^2 \langle H \rangle}{\partial A_z \partial A_z} = \kappa + (2\gamma_1 - \gamma_2)\left\langle Q_z^2 \right\rangle + (\gamma_1 + \gamma_2)\left\langle \, |\boldsymbol{Q}|^2 \, \right\rangle \\
&\qquad + 2g_a e_a - 4g_t\frac{e_t}{\sqrt{3}} - v_R, \\
\mathcal{D}_{xy} &= \frac{\partial^2 \langle H \rangle}{\partial A_x \partial A_y} = 2(\gamma_1 + \gamma_2)\langle Q_x Q_y \rangle - g_r e_6, \\
\mathcal{D}_{xz} &= \frac{\partial^2 \langle H \rangle}{\partial A_x \partial A_z} = 2(\gamma_1 + \gamma_2)\langle Q_x Q_z \rangle - g_r e_5, \\
\mathcal{D}_{yz} &= \frac{\partial^2 \langle H \rangle}{\partial A_y \partial A_z} = 2(\gamma_1 + \gamma_2)\langle Q_y Q_z \rangle - g_r e_4,
\end{aligned}$$

where $\langle Q_\lambda Q_{\lambda'} \rangle$ is given by Eq. (S13). To proceed further, we now consider the cubic and rhombohedral phases separately.

C. Cubic phase

In the cubic phase, $A_x = A_y = A_z = 0, \left\langle Q_x^2 \right\rangle = \left\langle Q_y^2 \right\rangle = \left\langle Q_z^2 \right\rangle = \psi_0, \langle Q_x Q_y \rangle = \langle Q_x Q_z \rangle = \langle Q_y Q_z \rangle = 0, e_a \neq 0, e_t = e_o = e_4 = e_5 = e_6 = 0, b_{\lambda\lambda'} = \delta_{\lambda\lambda'}$. Thus, the dynamical matrix is given as follows,

$$\begin{aligned}
&\mathcal{D}_{xx} = \mathcal{D}_{yy} = \mathcal{D}_{zz} = \overline{\kappa} + (5\gamma_1 + 2\gamma_2)\,\psi_0 + 2g_a e_a - v_R, \\
&\mathcal{D}_{xy} = \mathcal{D}_{xz} = \mathcal{D}_{yz} = 0.
\end{aligned}$$

The diagonalization of $\mathcal{D}_{\lambda\lambda'}$ gives a triply degenerate zone-boundary soft mode frequency,

$$\Omega_{R_4^+}^2 = \omega_{R_4^+}^2 + (5\gamma_1 + 2\gamma_2)\,\psi_0 + 2g_a e_a. \tag{S17}$$

Here, $\omega_{R_4^+} \equiv \sqrt{\overline{\kappa} - v_R}$ is the frequency of a purely harmonic model. ψ_0 are the local OP fluctuations in the cubic phase,

$$\psi_0 = \frac{1}{2\omega_R} \coth\left(\frac{\beta\omega_R}{2}\right), \tag{S18}$$

with $\omega_R = \sqrt{\Omega^2_{R_4^+} + v_R}$. The change in volume is given by the volumetric strain,

$$\frac{\Delta V}{V_0} = e_a = -\frac{3g_a}{C_a}\psi_0 - \frac{P}{C_a}, \tag{S19}$$

where V_0 is a reference volume.

We now calculate the Grüneisen parameter associated with R_4^+. From Eq. (S17), we find that the temperature and pressure dependence of $\gamma_{R_4^+}$ is entirely determined by the phonon energy,[R4]

$$\gamma_{R_4^+} = -\frac{\partial \ln \Omega_{R_4^+}}{\partial e_a} = -\frac{g_a}{\Omega^2_{R_4^+}}. \tag{S20}$$

Equations (S17)-(S19), determine self-consistently the temperature and pressure dependence of $\Omega_{R_4^+}$, and e_a.

D. Rhombohedral phase

In the r-phase, $A_x = A_y = A_z = A/\sqrt{3}, \psi_1 \equiv \psi_{xx} = \psi_{yy} = \psi_{zz}, \psi_4 \equiv \psi_{xy} = \psi_{xz} = \psi_{yz}, e_a \neq 0, e_o = e_t = 0, e_r \neq 0$ and,

$$b_{\lambda\lambda'} = \begin{pmatrix} \frac{1}{\sqrt{6}} & \frac{1}{\sqrt{2}} & \frac{1}{\sqrt{3}} \\ \frac{1}{\sqrt{6}} & -\frac{1}{\sqrt{2}} & \frac{1}{\sqrt{3}} \\ -\frac{2}{\sqrt{6}} & 0 & \frac{1}{\sqrt{3}} \end{pmatrix}. \tag{S21}$$

Thus, the dynamical matrix is given as follows,

$$\mathcal{D}_{xx} = \mathcal{D}_{yy} = \mathcal{D}_{zz} = \overline{\kappa} + (2\gamma_1 - \gamma_2)\left(\frac{A^2}{3} + \psi_1\right) + (\gamma_1 + \gamma_2)(A + 3\psi_1) + 2g_a e_a - v_R,$$
$$\mathcal{D}_{xy} = \mathcal{D}_{xz} = \mathcal{D}_{yz} = 2(\gamma_1 + \gamma_2)\left(\frac{A^2}{3} + \psi_4\right) - g_r e_r.$$

The diagonalization of $\mathcal{D}_{\lambda\lambda}$ together with the minimization of the free energy (S16) with respect to A gives the following result,

$$\Omega^2_{E_g} = \omega^2_{R_4^+} + (5\gamma_1 + 2\gamma_2)\left(\frac{A^2}{3} + \psi_1\right) + 2g_a e_a - 2(\gamma_1 + \gamma_2)\left(\frac{A^2}{3} + \psi_4\right) + g_r e_r, \tag{S22a}$$
$$\Omega^2_{A_{1g}} = \omega^2_{R_4^+} + (5\gamma_1 + 2\gamma_2)\left(\frac{A^2}{3} + \psi_1\right) + 2g_a e_a + 4(\gamma_1 + \gamma_2)\left(\frac{A^2}{3} + \psi_4\right) - 2g_r e_r, \tag{S22b}$$
$$\Omega^2_{A_{1g}} = 2(3\gamma_1 + 2\gamma_2)\frac{A^2}{3}, \tag{S22c}$$

e_a and e_r are volume and shear strains, respectively

$$e_a = -\frac{3g_a}{C_a}\left(\frac{A^2}{3} + \psi_1\right) - \frac{P}{C_a}, \tag{S23a}$$

$$e_r = \frac{g_r}{C_r}\left(\frac{A^2}{3} + \psi_4\right). \tag{S23b}$$

ψ_1 and ψ_4 are fluctuations of the OP in the r-phase,

$$\psi_1 = \frac{1}{3}\left(\frac{1}{2\omega_{A_{1g}}}\coth\left(\frac{\beta\omega_{A_{1g}}}{2}\right) + \frac{1}{\omega_{E_g}}\coth\left(\frac{\beta\omega_{E_g}}{2}\right)\right), \tag{S24a}$$

$$\psi_4 = \frac{1}{3}\left(\frac{1}{2\omega_{A_{1g}}}\coth\left(\frac{\beta\omega_{A_{1g}}}{2}\right) - \frac{1}{2\omega_{E_g}}\coth\left(\frac{\beta\omega_{E_g}}{2}\right)\right), \tag{S24b}$$

where $\omega_{E_g,A_{1g}} = \sqrt{\Omega^2_{E_g,A_{1g}} + v_R}$.

As mentioned above, the temperature and pressure dependence of the the Grüneisen parameters of the E_g and A_{1g} phonons are again entirely determined by their corresponding energies,

$$\gamma_{E_g,A_{1g}} = -\frac{\partial \ln \Omega_{E_g,A_{1g}}}{\partial e_a} = -\frac{g_a}{\Omega^2_{E_g,A_{1g}}}. \tag{S25}$$

Equations (S22)-(S24), determine self-consistently the temperature and pressure dependence of $\Omega_{E_g/A_{1g}}$, A, e_r and e_a.

1. *Classical Limit*

It is useful to consider the classical limit of the above results, as it allow us to derive analytical expressions for several relevant macroscopic quantities in terms of microscopic parameters. We consider the high-T cubic phase.

In the classical limit ($\beta\omega \ll 1$) and near the structural transition, $\psi_0 \simeq k_B T/v_R$, thus,

$$\frac{\Delta V}{V_0} \simeq \alpha_V T - \frac{P}{C_a}, \qquad \alpha_V = -\frac{3g_a k_B}{C_a v_R} \tag{S26}$$

where α_V is the coefficient of thermal expansion (CTE).

We find that he T and P dependence of $\Omega_{R_4^+}$ matches that of Landau theory, as expected,[R2]

$$\Omega^2_{R_4^+} = -\omega^2_{R_4^+} t, \tag{S27}$$

where $t = \frac{T - T_c(x,P)}{T_c(x,P)}$ is a reduced temperature and $T_c(x,P)$ is a pressure dependent transition temperature given as follows,

$$T_c(x,P) = T_c(x,0) + \frac{2g_a/C_a}{\gamma k_B/v_R} P, \tag{S28}$$

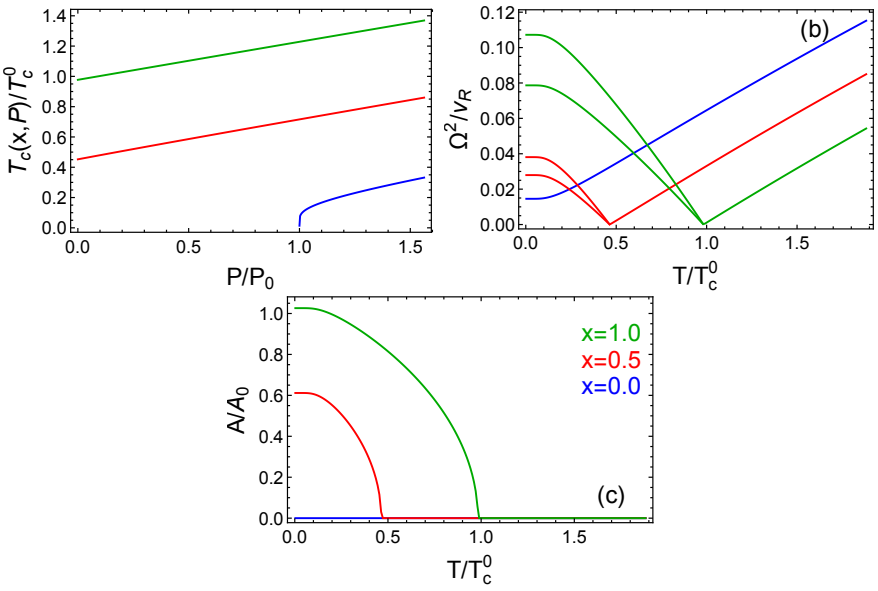

FIG. S1. Calculated (a) phase diagram (b) soft mode frequencies and (c) order parameter for $Sc_xTi_{1-x}F_3$.

where $T_c(x,0)$ is the transiton temperature at ambient pressure,

$$T_c(x,0) = \frac{-\omega^2_{R_4^+}}{\gamma k_B/v_R}, \tag{S29}$$

with $\gamma \equiv 5\gamma_1 + 2\gamma_2 - 6g_a^2/C_a$. Note that when there is a c-r transition, the high symmetry phase is unstable in the purely harmonic approximations and thus $\omega^2_{R_4^+} < 0$. The x dependence in $T_c\,(x,P)$ is through $\omega_{R_4^+}$, which in turn depends $\overline{\kappa}$, i.e., the lattice stiffness averaged over compositional disorder. Note that for $g_a > 0$, hydrostatic pressure destabilizes the c-phase. From Eq. (S28), we find a proportionality relation between the slope of the $T-P$ phase diagram and the CTE,

$$\frac{dT_c}{dP} = \frac{2g_a/C_a}{\gamma k_B/v_R} \propto -\alpha_V. \tag{S30}$$

We conclude the presentation of our model here.

III. MODEL PARAMETERS

The model parameters are given in Table I and were obtained from fits to experiments in $Sc_xTi_{1-x}F_3$.[R5,R6] We have assumed independent bimodal distributions for the stiffnesses $\mathcal{P}(\kappa_1,\kappa_2,...,\kappa_N) = \prod_{i=1}^N \mathcal{P}(\kappa_i)$, with $\mathcal{P}(\kappa_i) = x\delta(\kappa_i - \kappa_{\rm Ti}) + (1-x)\,\delta(\kappa_i - \kappa_{\rm Sc})$ and $\kappa_{\rm Ti/Sc}$ are the lattice stiffnesses of the pure compounds. With this choice, $\overline{\kappa} = x\kappa_{\rm Ti} + (1-x)\,\kappa_{\rm Sc}$. The resulting $T-P$ phase diagram, phonon frequencies and order parameter for several compositions are shown in Fig. S1.

TABLE I. Model parameters for $Sc_xTi_{1-x}F_3$.

κ_{Ti} [meV^2]	161
κ_{Sc} [meV^2]	173
v_R [meV^2]	173
γ_1 [meV^3]	21.8
γ_2 [meV^3]	−19.4
g_a [meV^2]	0.023
g_r [meV^2]	0.019
C_a [meV]	1.0
C_r [meV]	0.22

[R1] R. A. Cowley, Adv. Phys. **29**, 1 (1980).

[R2] E. Pytte, Phys. Rev. B **5**, 3758 (1972).

[R3] J. C. Slonczewski and H. Thomas, Phys. Rev. B **1**, 3599 (1970).

[R4] H. Volker, P. R. L. Welche, and M. T. Dove, J. Am. Ceram. Soc. **82**, 1793 (2004a).

[R5] S. U. Handunkanda, E. B. Curry, V. Voronov, A. H. Said, G. G. Guzmán-Verri, R. T. Brierley, P. B. Littlewood, and J. N. Hancock, Phys. Rev. B **92**, 134101 (2015).

[R6] C. R. Morelock, L. C. Gallington, and A. P. Wilkinson, Chem. Mater. **26**, 1936 (2014).